the plant journal

The Plant Journal (2020) 101, 420–441 doi: 10.1111/tpj.14534

RESOURCE

Single organelle function and organization as estimated from Arabidopsis mitochondrial proteomics

Philippe Fuchs[1,2,†], Nils Rugen[3,†], Chris Carrie[4], Marlene Elsässer[1,2,5], Iris Finkemeier[1], Jonas Giese[1], Tatjana M. Hildebrandt[3], Kristina Kühn[6], Veronica G. Maurino[7], Cristina Ruberti[1], Mareike Schallenberg-Rüdinger[5], Janina Steinbeck[1], Hans-Peter Braun[3,††], Holger Eubel[3,††], Etienne H. Meyer[6,††], Stefanie J. Müller-Schüssele[2,††] and Markus Schwarzländer[1,*††]

[1]*Institut für Biologie und Biotechnologie der Pflanzen (IBBP), Westfälische Wilhelms-Universität, Schlossplatz 7-8, 48143 Münster, Germany,*

[2]*Institut für Nutzpflanzenforschung und Ressourcenschutz (INRES), Rheinische Friedrich-Wilhelms-Universität Bonn, Friedrich-Ebert-Allee 144, 53113 Bonn, Germany,*

[3]*Institut für Pflanzengenetik, Leibniz Universität Hannover, Herrenhäuser Str. 2, 30419 Hannover, Germany,*

[4]*Department Biologie I - Botanik, Ludwig-Maximilians-Universität München, Grosshadernerstr. 2-4, 82152 Planegg-Martinsried, Germany,*

[5]*Institut für Zelluläre und Molekulare Botanik (IZMB), Rheinische Friedrich-Wilhelms-Universität Bonn, Kirschallee 1, 53115 Bonn, Germany,*

[6]*Institut für Biologie, Martin-Luther-Universität Halle-Wittenberg, Weinbergweg 10, 06120 Halle/Saale, Germany, and*

[7]*Institute of Developmental and Molecular Biology of Plants, and Cluster of Excellence on Plant Sciences (CEPLAS), Heinrich Heine University Düsseldorf, Universitätsstraße 1, 40225 Düsseldorf, Germany*

Received 12 June 2019; revised 23 August 2019; accepted 28 August 2019; published online 14 September 2019.
*For correspondence (e-mail markus.schwarzlander@uni-muenster.de).
[†]These authors contributed equally to this work.
[††]These authors contributed equally to this work.

In memory of Axel Brennicke (1953–2017).

SUMMARY

Mitochondria host vital cellular functions, including oxidative phosphorylation and co-factor biosynthesis, which are reflected in their proteome. At the cellular level plant mitochondria are organized into hundreds of discrete functional entities, which undergo dynamic fission and fusion. It is the individual organelle that operates in the living cell, yet biochemical and physiological assessments have exclusively focused on the characteristics of large populations of mitochondria. Here, we explore the protein composition of an individual average plant mitochondrion to deduce principles of functional and structural organisation. We perform proteomics on purified mitochondria from cultured heterotrophic Arabidopsis cells with intensity-based absolute quantification and scale the dataset to the single organelle based on criteria that are justified by experimental evidence and theoretical considerations. We estimate that a total of 1.4 million protein molecules make up a single Arabidopsis mitochondrion on average. Copy numbers of the individual proteins span five orders of magnitude, ranging from >40 000 for Voltage-Dependent Anion Channel 1 to sub-stoichiometric copy numbers, i.e. less than a single copy per single mitochondrion, for several pentatricopeptide repeat proteins that modify mitochondrial transcripts. For our analysis, we consider the physical and chemical constraints of the single organelle and discuss prominent features of mitochondrial architecture, protein biogenesis, oxidative phosphorylation, metabolism, antioxidant defence, genome maintenance, gene expression, and dynamics. While assessing the limitations of our considerations, we exemplify how our understanding of biochemical function and structural organization of plant mitochondria can be connected in order to obtain global and specific insights into how organelles work.

Keywords: plant mitochondrion, single organelle, proteomics, intensity-based absolute quantification, oxidative phosphorylation, TCA cycle, antioxidant defence, cofactor synthesis, mitochondrial genome, RNA editing, mitochondrial fission, *Arabidopsis thaliana*.

INTRODUCTION

Mitochondria are central to complex life. Their evolutionary, genetic, biophysical, biochemical, and cell biological characteristics have been studied intensely. However, the resulting views of the organelle have remained remarkably separated between disciplines in several cases. Mitochondria were recognized early as organelles that exist as multiple individual entities in cells (Altmann, 1890). Those entities were later identified as the location of respiration, based on morphological considerations (Kingsbury, 1912), and dissected in their architecture by electron microscopy, and, more recently, super-resolution microscopy techniques (Sjostrand, 1953; Jakobs and Wurm, 2014; Chen *et al.*, 2018). Edmund V. Cowdry recognized the intrinsic limitation of pure morphological investigations as early as 1924 by pointing out that

> it is quite obvious that the investigation of mitochondria will never achieve the usefulness which it deserves as an instrument for advance in biology and medicine until we know much more of their chemical constitution as the only accurate basis for interpretation of our findings. In other words, we must wait up on the slow development of direct, quantitative cellular chemistry. (Cowdry, 1924)

In parallel, mitochondrial functions, such as their respiratory or biosynthetic features, were analysed across large numbers of mitochondria in organisms and tissues, or isolated from those sources (Utter *et al.*, 1958; Ohnishi and Hagihara, 1964; Weiss *et al.*, 1970; Werner and Neupert, 1972). The fundamental divide between cell biological and biochemical approaches to mitochondria has left a void at the centre of organelle biology, leaving the question open of how exactly the individual mitochondrion carries out its functions as a physically discrete unit.

How the individual mitochondrion, as the smallest unit of mitochondrial populations in cells, works is relevant across eukaryotic organisms. Several organisms contain extensive mitochondrial networks (Hoitzing *et al.*, 2015) resulting in a situation of a single cell containing only a few large mitochondria or even a single physically discrete mitochondrion. Examples are mitochondria in yeast, trypanosomes or several mammalian cell types (de Souza *et al.*, 2009; Rafelski, 2013; Zamponi *et al.*, 2018; Vincent *et al.*, 2019). At the opposite end of this spectrum, small, highly fragmented mitochondria are present, for instance, in mammalian neurons and flowering plant cells. Cells of flowering plants, such as the reference organism *Arabidopsis thaliana*, typically contain several hundred of discrete organelles per cell, which are connected over time by fusion and fission (Sheahan *et al.*, 2005). The organizational structure of plant mitochondria has been described as a 'discontinuous whole' (Logan, 2006), to emphasize that the organelles form a continuous network that does not exist in space but over time. However, nearly all mitochondrial function occurs at the level of the individual mitochondrion and is constrained by the physical properties of the individual unit.

A realistic understanding of the processes that occur at the single organelle level requires *in vivo* analysis. This has become possible for specific parameters through fluorescent sensors, and has provided initial insights into heterogeneity in composition and function between single mitochondria, e.g. with respect to mtDNA content and bioenergetics (Arimura *et al.*, 2004b; Schwarzländer *et al.*, 2012). Yet, imaging-based approaches to explore the properties of individual mitochondria remain cumbersome, are typically limited to only a small set of parameters and leave a large proportion of mitochondrial functions inaccessible. Very recently, an imaging-based approach was used to estimate stoichiometry and protein copy numbers in carboxysomes (Sun *et al.*, 2019) raising hopes that analogous approaches may become available for other organelles in the future.

The development of increasingly sensitive and sophisticated proteomic approaches has allowed the identification of proteins in mitochondrial extracts and to infer functional characteristics of mitochondria (Kruft *et al.*, 2001; Millar *et al.*, 2001; Heazlewood *et al.*, 2004). Also a limited number of quantitative proteomic datasets of plant mitochondria have been reported (Nelson *et al.*, 2013; Mueller *et al.*, 2014; Salvato *et al.*, 2014; Wagner *et al.*, 2015; Senkler *et al.*, 2017) and relative protein abundances have been linked to specific mitochondrial pathways (Taylor *et al.*, 2011). Generating proteomic datasets from a single mitochondrion of any organism remains impossible due to technical constraints. Important insights into the proteome of a single mitochondrion come from a recent study in yeast (Morgenstern *et al.*, 2017). High quality quantitative proteomic datasets allowed the extraction of absolute copy numbers of the individual mitochondrial proteins under the assumption that each yeast cell hosts a single mitochondrion. The fragmented nature of plant mitochondria, with hundreds of small and discrete units per cell adds a further layer of complexity. An elegant first step towards the protein inventory of a single plant mitochondrion has recently been taken through a theoretical appraisal (Møller, 2016).

Our motivation to explore the composition of a single mitochondrion is based on the question if new insights into organelle biology can be obtained by applying the geometrical constraints under which the individual mitochondria function to biochemical data generated from a population of mitochondria. Normalization of quantitative proteomic data allows scaling down from the population

to the averaged individual, which may already deliver decisive benefits.

In this article, we explore the proteomic makeup of a single mitochondrion and what that might imply for its structure and function as an individual unit. We use shotgun proteomics of isolated mitochondria from heterotrophic Arabidopsis cell suspension culture in combination with intensity-based absolute quantification (iBAQ). We normalize the proteomic dataset to derive average copy numbers of individual proteins in a single mitochondrion using reasonable assumptions based on experimental evidence about the physical properties of a typical plant mitochondrion. We make use of the protein copy numbers per mitochondrion to explore the potential added value of considering the single organelle to gain meaningful insights into plant mitochondrial properties and processes. We unite expertise from several current fields of plant research to explore the implications of a single organelle perspective on a range of specific biological questions. We develop hypotheses and devise several thought experiments, based on available data, to synthesize an original perspective that illustrates how individual mitochondria operate. The approach exemplifies a strategy that may be used also for other organisms, cells and organelles.

RESULTS AND DISCUSSION

Towards the protein inventory of a single mitochondrion

A single mitochondrion is made up by about 1.4 million proteins. We aimed at estimating the total protein number per single mitochondrion. This requires assumptions about mitochondrial size and shape, both of which are variable in plant mitochondria. Based on literature micrographs, our own experience with live fluorescence microscopy as well as transmission electron microscopy of *A. thaliana* mitochondria (Figure 1a), a sphere of 0.8 μm in diameter represents a reasonable approximation of an average mitochondrion from a living heterotrophic Arabidopsis cell (de Virville *et al.*, 1998; Logan and Leaver, 2000; Eubel *et al.*, 2007). Most Arabidopsis mitochondria are spherical to bean-shaped within a diameter range of 0.4–2.0 μm, with the exception of slender, extended individuals, which are typically underrepresented. Mitochondrial density previously measured experimentally at 1.2 g ml^{-1} (Glas and Bahr, 1966), allows estimating the weight of a single hydrated plant mitochondrion of 0.8 μm in diameter at 322 fg (see Dataset S1, worksheet #2). The dry mass contribution to hydrated mitochondrial weight was determined at 26–35%, but was subsequently criticized as a gross underestimation (Glas and Bahr, 1966; Berthet and Baudhuin, 1967). Assuming 25% protein content, which is justified by the additional presence of lipids, metabolites, RNA and DNA, a single mitochondrion contains 80.4 fg of protein (Dataset S1, worksheet #2).

To estimate how many protein copies a mitochondrion is comprised of, we calculated the abundance-adjusted weight of an average protein in our proteomic samples (as introduced below), equalling 38 350 Da (6.37×10^{-20} g), closely reflecting the values retrieved from the SUBAcon database (39 247 Da) (Hooper *et al.*, 2014) (Dataset S1, worksheet #4). Considering that an N-terminal targeting peptide of a large proportion of proteins, encoded in the nuclear genome, is proteolytically cleaved after import, we subtracted 3514 Da (abundance-weighted average mitochondrial target peptide size, corrected for frequency of occurrence, see Dataset S1, worksheet #5) (Kmiec *et al.*, 2014; Ghifari *et al.*, 2019). Accordingly, a mass of 34 836 Da (5.78×10^{-20} g) was estimated for a mature mitochondrial protein on average, resulting in 1 390 777 protein molecules that constitute a single mitochondrion. This is in line with previous estimations (10^6 protein copies for a small mitochondrion; 1.6×10^6 for a mitochondrion of the size considered here) derived from a different set of assumptions (Møller, 2016).

Intensity-based quantitative proteomics to estimate protein copy numbers per mitochondrion. To exemplify our approach, we chose isolated mitochondria from Arabidopsis dark-cultured cell suspensions for shotgun proteomics. The cell suspensions provide the technical advantage of fast growth and low contamination with photosynthetic plastid proteins. They do not represent any specialized tissue and are not synchronized for cell cycle progression, minimizing bias from specialized functions or a dominating effect of biogenesis. While specific functions, such as the support of photosynthesis, are unlikely to be represented by this material, it will be straightforward to adjust the approach to any other source of mitochondria.

Four biological replicates from separate mitochondrial protein isolations were analyzed by liquid chromatography coupled with tandem mass spectrometry (LC-MS/MS). At least one unique peptide was required for a protein to be considered as identified. An intensity-based absolute quantification (iBAQ) score was used as a quantitative estimate for each identified protein, for which only unique peptides and razor peptides were taken into account (Arike *et al.*, 2012). We normalized the iBAQ scores against the sum of all iBAQ values in each replicate, calculated the median iBAQ score per protein across the four replicates and re-normalized against the sum of all iBAQ scores. The resulting normalized median iBAQ scores indicate the fraction of the quantitative contribution of each protein to the proteome. Multiplication of this score for each protein by the total number of protein molecules per single mitochondrion (1 390 777; see above) provided an estimate of the copy number of each protein species per mitochondrion (Figure 1a). This approach provides meaningful estimates of protein copy number across the proteome overall, but is

Figure 1. The proteome of a single mitochondrion.
(a) Overview of our approach summarizing the proteomics and the calculations made to obtain copy numbers. Steps marked with blue background represent assumptions; all others are based on experimental findings, physical constraints and calculations. See Dataset S1, worksheet #2, for all calculation details. The electron micrograph was obtained from a mitochondrial preparation from heterotrophic Arabidopsis cell suspension culture. Liquid chromatography coupled with tandem mass spectrometry (LC-MS/MS); Intensity-Based Absolute Quantification (iBAQ).
(b) Subcellular location of identified proteins. In total 2934 protein species were identified and classified according to their likely subcellular location based on SUBAcon (Hooper *et al.*, 2014). The cumulated copy number of all protein species allocated to a subcellular compartment is provided in brackets and displayed as a percentage of the total copy number of all proteins.
(c) Functional meta-categories for 917 proteins with mitochondrial localisation as identified by SUBAcon (finer classification into functional sub-categories is shown in Table S1); Unknown function protein (UFP).

(a)

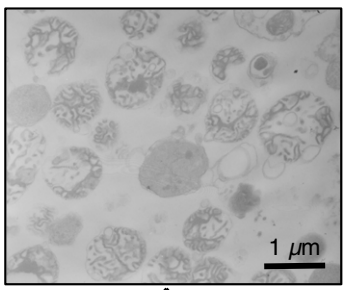

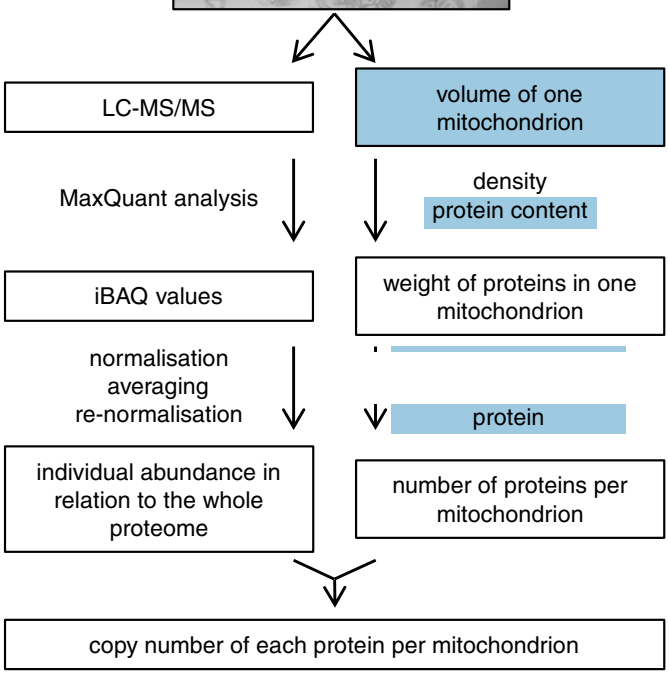

(b)

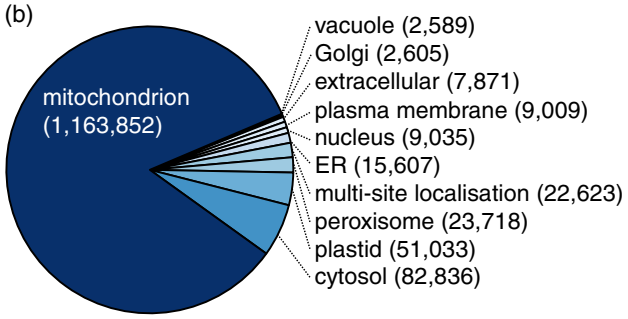

(c)

functional meta-category	copy number	protein species	rel. abundance
ATP production and export	557,063	141	47.9%
protein import, synthesis, modification and turnover	221,372	365	19.0%
metabolism	139,798	123	12.0%
transport	125,845	45	10.8%
UFP	60,903	193	5.2%
other minor groups	58,871	50	5.1%
total	1,163,852	917	100%

limited by the intrinsic shortcomings of proteomic analysis of biological samples and iBAQ quantitation, such as the individual biochemical peptide properties affecting ionisation and detection characteristics (Schwanhäusser *et al.*, 2011; Fabre *et al.*, 2014; Krey *et al.*, 2014). To exemplify the principle in the following sections we treat the calculated copy numbers from the datasets as precise values.

Critical appraisal of the single mitochondrion proteome dataset. In total, 2934 protein species were identified and quantified across the four biological replicates (Dataset S1, worksheet #1). More than two-thirds of these were detected in all four samples (Figure S1a), indicating that the dataset is coherent with respect to both protein content and technical reproducibility.

Organelles isolated from disrupted cells often contain proteins attributed to other cellular components, which may reflect contaminations or shared components. We used the SUBAcon algorithm (Hooper *et al.*, 2014) which unambiguously assigned 2799 proteins to a single cellular location, based on weighted experimental evidence and predictions. One third of these (917 proteins) are annotated as mitochondrial, while most of the remaining proteins were annotated as plastidic (597 proteins) or cytosolic (564 proteins, Figure S1b). Protein abundance (as deduced from normalized iBAQ values; Dataset S1, worksheet #1) revealed that 84% of the protein content in the mitochondrial isolates are of mitochondrial origin (1 163 852 copies out of 1 390 777 copies in total; Figure 1b), which matches in range the purity of isolated Arabidopsis mitochondria used for quantitative proteomics reported previously (Klodmann *et al.*, 2010; Senkler *et al.*, 2017).

One of the four replicates contained a higher amount of plastid contamination as indicated by the strongly increased abundance of the marker proteins RbcL, AccD, ClpP1, and Rps11, which are encoded by the plastid genome (Dataset S1, worksheet #1). We consciously decided to use the full dataset without applying additional selection criteria, because many mitochondrial proteins are expected to be present at low abundance and would be lost if more stringent parameters were applied. In addition, the use of median instead of mean for our calculations of the normalized iBAQ values largely balanced the effects originating from an individual outlier (i.e. one replicate with higher contamination levels). For the specific goals pursued here limiting the risk of excluding mitochondrial proteins of low abundance outweighs the benefit of stringent exclusion of contaminants. Another limitation is the inherent incompleteness of proteomic datasets. Thus, several mitochondrial proteins, such as the intron maturase MatR or the OXPHOS subunit Atp9, which are encoded in the mitochondrial genome, were not identified. Although they may not be expressed (or very lowly) in the cells we analysed, their absence in our dataset is more likely due to their biochemical properties preventing their identification by mass spectrometry. Out of the different groups of mitochondrial proteins, the oxidative phosphorylation (OXPHOS) complexes are particularly prone to underestimation partly because they are enriched in protein subunits with unfavourable properties for mass spectrometry, such as small size and high hydrophobicity.

Considerations about the mitochondrion as an individual

Almost half of the mitochondrial proteome serves cellular ATP provision. When the 917 mitochondrial protein species are broadly classified according to their annotated functions (Table S1; Figure 1c; Figure S1c,d; Hooper *et al.*, 2014), the group of proteins involved in ATP production and transport makes up 557 063 copies, which is almost 48% of the total mitochondrial protein content. The 97 proteins involved in OXPHOS (105 when complex II is included) contribute most of the copies. Interestingly, 53 944 protein copies (10% of copies within this group) belong to only five ATP transporters (AAC1, AAC2, AAC3, APC2, ADNT1), mirroring the extremely high ATP fluxes that a mitochondrion is able to maintain. The combined copy number of all remaining mitochondrial transporters identified for the inner membrane (IMM) and outer membrane (OMM; 125 845 copies in total) belong to distinctively more protein species (45 protein species).

Protein import, synthesis, modification and turnover, are carried out by 221 372 protein molecules (19% of the total mitochondrial protein content, Figure 1c). The high number of 365 protein species in this meta-group that includes the functional groups 'protein import', 'RNA processing', 'protein synthesis' and 'protein fate' (Table S1), is mainly due to the high number of proteins related to RNA processing (135 protein species), most of which are pentatricopeptide repeat (PPR) proteins. Metabolism not related to cellular respiration uses only 139 798 molecules (12% of the mitochondrial protein content) and is mainly related to amino acid metabolism (44 of 123 protein species in this meta-group).

The makeup of the outer and inner mitochondrial membranes is dominated by few protein species. The mitochondrion is delimited by a double membrane system and each membrane contains a specific set of proteins. The protein with the highest copy number in the mitochondrion is the Voltage-dependent anion channel 1 (VDAC1: 44 381 copies), which resides in the OMM and constitutes the main passage between the cytosol and the intermembrane space (IMS) for a large variety of compounds (Colombini, 2004). In a single Arabidopsis mitochondrion, 80 760 monomers of the five VDAC isoforms (VDAC1–5) are present, which equals a density of 40 167 VDAC channels per μm^2 (OMM surface: 2.0 μm^2) (Dataset S2, worksheet #1). Assuming that the dimensions of the Arabidopsis VDACs are similar to

those found for the human VDAC crystal structure (Bayrhuber *et al.*, 2008; 8.5 nm^2 lipid-displacing area), 34.2% of the OMM surface consist of VDAC proteins (Figure 2; Dataset S2, worksheet #1), making VDACs a major building block of the OMM. Considering that VDAC conductance is regulated (Zizi *et al.*, 1994; Hodge and Colombini, 1997; Mlayeh *et al.*, 2010), the VDAC proteins not only provide a high degree of permeability to the OMM, but also effectively functionalise the membrane to act as a conditional *nano-sieve*. Gating of metabolite fluxes by VDACs is likely to play an important regulatory role to adjust organelle metabolism, physiology and volume (Liu and Colombini, 1992). *Pits* and *in-plane subunits* of proteins that occur at sufficiently high density to adopt crystalline array

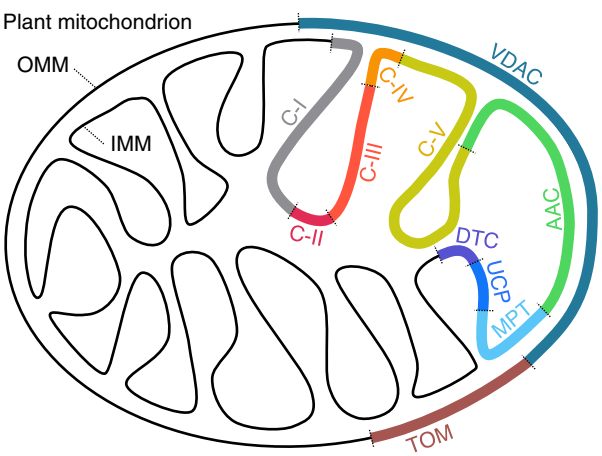

Protein family/complex	area of OMM
VDAC	34.2%
TOM	12.1%
Protein family/complex	**area of IMM**
Complex I (C-I)	5.0%
Complex II (C-II)	0.8%
Complex III (C-III)	2.7%
Complex IV (C-IV)	1.2%
Complex V (C-V)	8.4%
AAC	6.2%
MPT	2.5%
UCP	1.0%
DTC	0.8%
remaining proteins	~1.1%

Figure 2. Proportions of mitochondrial membrane areas constituted by individual protein families.
Schematic representation of the outer mitochondrial membrane (OMM) and the inner mitochondrial membrane (IMM) of a typical plant mitochondrion in a 1:3 ratio (membrane area represented as lines). Colour-coded membrane segments represent the proportional constitution of OMM or IMM by highly abundant protein families and protein complexes in % of total membrane area occupied as shown in the table inset. VDAC (voltage-dependent anion-selective channel protein), TOM (translocase of the outer membrane), C-I (NADH:ubiquinone oxidoreductase), C-II (succinate dehydrogenase), C-III (cytochrome bc_1 complex), C-IV (cytochrome *c* oxidase), C-V (ATP-synthase), AAC (ADP/ATP carrier), MPT (mitochondrial phosphate carrier protein), UCP (uncoupling protein), DTC (mitochondrial dicarboxylate/tricarboxylate carrier).

organisation were already found in early electron micrographs and by X-ray diffraction of plant OMM preparations (Parsons, 1965; Mannella and Bonner, 1975; Mannella, 1982). They can be retrospectively identified as VDAC. A density of 20 000 molecules per μm^2 OMM was calculated by Mannella and Bonner, 1975, corresponding to 40 000 VDAC proteins per mitochondrion, or 20% of OMM for the mitochondrial dimensions adopted here. Both estimates (34.2% and 20%) turn out similar, considering that they are derived from independent approaches and different assumptions. A second major constituent of the OMM is the Translocase of the Outer Membrane (TOM) complex that covers an additional 12.1% of the OMM surface area (Figure 2; Dataset S2, worksheet #6) and is discussed in further detail in the next section.

In contrast to the domination of the OMM by the protein families of VDAC and TOM, the IMM protein inventory is made up by a large number of different proteins of which a large proportion groups into the OXPHOS complexes (17 258 complexes; Dataset S2, worksheet #2) and carrier proteins (97 980 copies) (Dataset S2, worksheet #3; Figure 2). Assuming a OMM:IMM ratio of 1:3 as reported for rat liver mitochondria (Schwerzmann *et al.*, 1986), complex I (~120 nm^2 lipid-displacing area; Zickermann *et al.*, 2015) alone constitutes 5% of the IMM (6 μm^2), while complex II (~16 nm^2 lipid-displacing area; Sun *et al.*, 2005), III_2 (~50 nm^2 lipid-displacing area; Zhang *et al.*, 1998) and IV (~38 nm^2 lipid-displacing area; Dudkina *et al.*, 2011) together add up to another 4.7% (0.8%, 2.7% and 1.2%, respectively) (Dataset S2, worksheet #2). The estimated mitochondrial electron transport chain (ETC) complex density ranges for the complexes I to IV (413, 523, 542, and 318 complexes per μm^2, respectively) are in general agreement with previous reports for mammalian mitochondria (277, 535, 812, and 1880 complexes per μm^2, respectively) (Gupte *et al.*, 1984). Conceivably, packing high amounts of bulky ETC complexes, particularly complex I, into the membrane impacts on the overall IMM architecture. This concept is well-established for ATP-synthase dimers, which introduce the curvature required for cristae formation (Dudkina *et al.*, 2005; Davies *et al.*, 2012; Hahn *et al.*, 2016). In our dataset, the total area of the ATP-synthase membrane-integral part amounts to 8.4% area of the IMM, which nearly equals the area composed of complexes I–IV (9.7% of IMM area). Overall the OXPHOS complexes make up 18.1% of the IMM, which is in line with ATP production as a defining mitochondrial function (Figure 2; Dataset S2, worksheet #2).

OXPHOS relies on bulk substrate availability in the mitochondrial matrix, which needs to be supplied from the cytosol by high flux rates through IMM carriers. The necessity for high transport capacity is mirrored by high copy numbers of transporters mediating the exchange of ADP/ATP, Pi/H$^+$, di- and tricarboxylates and the uncoupling of

the H^+-gradient at 53 065 (mitochondrial ADP/ATP carrier 1–3; AAC1–3), 21 325 (mitochondrial phosphate transporter 2 and 3; MPT2 and MPT3), 6836 (mitochondrial dicarboxylate/tricarboxylate carrier, DTC) and 8595 (uncoupling proteins 1 and 3; UCP1 and UCP3) copies (Dataset S2, worksheet #3). These transporters make up 10.5% of IMM area assuming a lipid-displacing area of ~7 nm^2 as estimated from the bovine AAC crystal structure (Pebay-Peyroula *et al.*, 2003) (AAC 6.2%, MPT 2.5%, DTC 0.8% and UCP 1%; Figure 2; Dataset S2, worksheet #3). In contrast to the transporters that mediate the bulk fluxes of energy metabolism, all remaining identified carriers together amount to 1.1% of IMM area. Note that this is based on the curated list of IMM transporters in Dataset S2 (worksheet #3), and not the global, but less precise, SUBAcon classification, which includes proteins, such as GET3c or MICU that are not membrane transporters. In total, the OXPHOS and carriers account for ~30% of the IMM area, corresponding to 41.4% of the IMM weight (Dataset S2, worksheet #4), which is about half of what has been previously estimated (~80 weight-%) (Krauss, 2001). While the concept of proteins dominating the makeup of the IMM is supported by our estimations, the difference to previous numbers is likely due to the underestimation of OXPHOS proteins by the MS-based approach. This effect may be illustrated taking complex I as an example, which is made up of a matrix arm and a membrane arm at a 1:1 stoichiometry. Averaging the number of matrix arm proteins results in 3932 matrix arm copies, but averaging the number of membrane arm proteins results in only 1841 membrane arm copies. There is no experimental indication, however, of a significant amount of unassembled matrix arm subunits in the mitochondrion (Meyer *et al.*, 2007). Instead matrix arm proteins are typically found in the membrane fraction, i.e. assembled with the membrane arm and set in stoichiometry. This inconsistency suggests that the copy numbers of the membrane arm proteins are systematically underestimated by the mass spectrometry approach. The number of complex I particles per mitochondrion may be more realistically estimated based on the matrix arm only, which would increase the estimation from 2491 complex I copies (averaged across all subunits) to 3932 complex I copies (average of matrix arm subunits only) (Dataset S3, worksheet #2). An analogous effect is to be expected for other OXPHOS complexes, but it is hard to account for this effect systematically due to the individual biochemical properties of the complex subunits involved. The rough assumption of doubling the OXPHOS complex copy numbers increases the protein area of the IMM to 48%, corresponding to 62% of the membrane weight, which closes the gap to previous reports using independent approaches (Krauss, 2001).

A maximum of 18 crista sheets can be stacked in the typical Arabidopsis mitochondrion, based on the dimensions of the OXPHOS complexes (here specifically complex I and complex V) (Dataset S2, worksheet #5). Assuming that those cristae are organized as flat sheet structures that span the entire available diameter of the matrix, the summed-up length of the cristae ridges, where rows of ATP synthase dimers provide curvature (Blum *et al.*, 2019), adds up to 32.5 μm. Considering a diameter of about 10 nm per ATP synthase dimer in the row of dimers (Zickermann *et al.*, 2015), 3253 dimers are required to constitute the cristae ridges. This requirement matches the number of ATP synthase molecules present in the single mitochondrion (6426 monomers, 3213 dimers) (Dataset S3, worksheet #2). This remains a rough estimate since the cristae may adopt different sizes and more complex shapes, which would then decrease or increase, respectively, the number of dimers required. The presence of the 18 crista sheets is an upper limit, since it would leave insufficient space for large protein complexes, such as the pyruvate decarboxylase complex (PDC), 2-oxoglutarate dehydrogenase complex (OGDC) and the glycine decarboxylase complex (GDC), in the matrix (discussed in the sections on TCA cycle and GDC). Furthermore, 18 cristae would result in an IMM surface area of 12 μm^2, or an IMM:OMM surface area ratio of 6:1 instead of 3:1, as used for the estimations above (Schwerzmann *et al.*, 1986). In the presence of less cristae, a surplus of ATP-synthase molecules may exist as monomers that do not introduce membrane curvature (Blum *et al.*, 2019), or as dimers to introduce more complex cristae structures.

The protein import machinery could double the mitochondrial proteome in under 7 h. Of all mitochondrial protein copies, 12% are involved in protein import and protein fate, including maturation, folding, and degradation (221 372 protein copies; Figure 1c; Table S1). The components of the import apparatus are of particular importance since the vast majority of mitochondrial proteins are encoded by nuclear genes, synthesized in cytosolic ribosomes, and must be imported.

The main entry gate into mitochondria is the translocase of the outer membrane (TOM) complex and almost all proteins entering mitochondria must pass through it. The TOM complex is by far the most abundant import complex found in a single mitochondrion with 8139 TOM40 copies (Dataset S2, worksheet #6). Previous work on mammalian and yeast mitochondria have demonstrated that the TOM complex is triangular (containing 3 TOM40 channels) measuring 14.5 nm on edge and that between 8 and 14 TOM complexes cluster together in assemblies of approximately 30–40 nm in diameter (Model *et al.*, 2008; Wurm *et al.*, 2011). Assuming these values are similar for plant TOM complexes, a single plant mitochondrion contains 247 TOM complex clusters on average (assuming 11 TOM complexes per cluster), accounting for 12.1% of the OMM surface area as noted above (Dataset S2, worksheet #6;

Figure 2). These numbers match previous observations in yeast, which contains approximately 100 active import sites per μm^2 of OMM surface area (Gold *et al.*, 2014).

The two translocases of the inner membrane, the TIM23 and TIM22 complexes, are present at much lower numbers. Assuming that both complexes exist as dimers (Bauer *et al.*, 1996), only 175 TIM22 complex dimers (349 copies of TIM22) and 370 TIM23 complex dimers (740 copies of TIM17 and 852 copies of TIM23) are present per mitochondrion (compared to the 2713 TOM complexes) (Figure S2). In yeast, the stoichiometry of TOM40:TIM23:TIM22 proteins was calculated to be 5:1:0.2 (Sirrenberg *et al.*, 1997), in plant mitochondria we found a very similar stoichiometry 7.3:1:0.5. TOM complexes are found in excess over the inner membrane translocases and this may reflect the fact that the TOM complexes must import, in addition to proteins of the inner membrane and the matrix, proteins destined for the OMM and the IMS. TIM22 is only present at 349 copies per mitochondrion, while one of the many TIM22 substrates, the ATP/ADP carrier 1 protein (AAC1), is present at 39 984 copies. The TIM23 complex imports proteins containing pre-sequences, equalling approximately 70% of protein copies (973 544 copies) per mitochondrion. How long would it take one mitochondrion to double the copy number of all TIM23 substrates? Assuming a translocation rate of 40 amino acids per second (based on Sec pathway measurements in bacteria, (Fessl *et al.*, 2018), an average protein length of 353 amino acids and 370 active import sites per mitochondrion (assuming that the TIM23 complex is the limiting step), it would take approximately 6 h and 27 min to double the number of TIM23 substrate proteins in a single mitochondrion.

Composition and function of the OXPHOS system. The OXPHOS system of plants consists of the complexes I–V, cytochrome *c*, the alternative oxidase (AOX) and alternative NAD(P)H dehydrogenases (NDs) (Meyer *et al.*, 2019). Overall, 115 proteins that represent subunits of OXPHOS components were identified in the course of a recent complexome profiling approach in Arabidopsis and additional 21 proteins were identified by other investigations (Senkler *et al.*, 2017 and discussion within). If isoforms are subtracted, the Arabidopsis OXPHOS system—according to current knowledge—consists of 105 distinct protein species. Only three of these proteins are not covered by our proteome datasets (the SDH8 subunit of complex II and the c-subunit of the ATP synthase complex, both of which are very small and hydrophobic, and the AOX1B protein; Dataset S3, worksheet #2). Copy numbers of proteins forming part of the same protein complex vary to a degree (Dataset S3, worksheet #2), which may be due to biological reasons (e.g., multiple copies of some subunits per complex [e.g., α- and β-subunit of complex V], non-assembled subunits) or technical reasons (e.g., dependence of the iBAQ score on the hydrophobicity of a protein). Average copy numbers of OXPHOS components were calculated by averaging copy numbers of all the identified subunits (corrected for specific subunits if they are present in more than one copy per complex) (Dataset S3, worksheet #2). The result likely represents a lower estimate of the number of OXPHOS complexes. An account of the limits of this approach is provided above in the section "*Critical appraisal of the single mitochondrion proteome dataset*".

The ATP synthase (complex V; 6426 particles per mitochondrion) and complex III (6537 complex III monomers, corresponding to 3268 complex III dimers) are the most abundant OXPHOS components, which correlates well with results from blue native PAGE (Senkler *et al.*, 2017). About 2491 copies of complex I, 3156 copies of complex II and 1916 copies of complex IV are present per mitochondrion. These numbers explain why supercomplex formation of complex I and dimeric complex III leads to drastic reduction of monomeric complex I particles, while complex III dimers remain abundant (Dudkina *et al.*, 2005). The copy number of cytochrome *c* (2252) lies in between the copy numbers of dimeric complex III and complex IV. Complex IV of plants can also form part of respiratory supercomplexes together with dimeric complex III or dimeric complex III plus monomeric complex I (Eubel *et al.*, 2004). Respiratory supercomplexes that include the complexes I, III_2 and IV are also designated "respirasomes", because they can autonomously carry out the entire reaction of the ETC (assuming cytochrome *c* and ubiquinone are present). The copy number of complex IV in a single mitochondrion of Arabidopsis suggests that complex IV is limiting respirasome formation in plant mitochondria. There is a current consensus that supramolecular assemblies of respiratory supercomplexes and singular (monomeric) respiratory complexes co-exist under *in vivo* conditions and that the degree of supercomplex formation varies depending on physiological conditions of plant cells (Ramírez-Aguilar *et al.*, 2011). In total, 222 136 proteins form part of the four *classical* protein complexes of the respiratory chain (complexes I–IV), 52.9% (117 427) belonging to complex I. In Arabidopsis, complex I contains a carbonic anhydrase (CA) domain that includes gamma-type CA subunits (Fromm *et al.*, 2016b). This domain consists of three CA subunits of the five known plant CA/CAL proteins (CA1, CA2, CA3, CAL1 and CAL2) in combinations that are not precisely defined so far (Fromm *et al.*, 2016b). With the realistic assumption that these five proteins have similar biochemical properties and therefore their copy numbers can be interpreted in term of stoichiometry, our results show that the CA2 protein is clearly the most prominent CA/CAL protein (47% of all CA/CAL proteins). Summed up copy numbers for CA1 and CA3 only account for 31% and the ones for CAL1 and CAL2 for 22%. This provides a plausible

explanation for the particularly drastic reduction of complex I in mutants lacking CA2 (Wang *et al.*, 2012; Fromm *et al.*, 2016a).

Assuming a respiratory activity of 200 nmol O_2 min^{-1} mg $protein^{-1}$ that is typical for isolated Arabidopsis mitochondria (Eubel *et al.*, 2007; Wagner *et al.*, 2015) and an ADP/O ratio of 2.5, we estimated that a single mitochondrion produces 968 658 ATP molecules per second, corresponding to 151 ATP molecules by each of the 6426 ATP synthase complexes (Dataset S2, worksheet #7). This synthesis rate corresponds to a rotation rate of ATP synthase of 50 sec^{-1}, which is consistent in range with the 130 sec^{-1} measured for the ATP hydrolysis activity of a prokaryotic ATP-synthase at saturating ATP supply (Yasuda *et al.*, 2001). Assuming that all export of the ATP that the mitochondrion synthesizes is mediated by AAC1–3, each of the 53 065 AAC protein copies (Dataset S2, worksheet #3) needs to transport 18 ATP molecules per second. The combined activities of the 6426 ATP-synthase motors deliver 103 fW of power per mitochondrion (assuming $\Delta G(ATP)$ at -64 kJ mol^{-1} under physiological conditions). This means that less than a 2-cl shot glass worth of respiring mitochondria (18.2 ml) turn over the equivalent of the power consumption of a modern 7W LED, that replaces the traditional 60W light bulb (Dataset S2, worksheet #8).

TCA cycle proteins make up over 80% of the matrix protein volume. The tricarboxylic acid (TCA) cycle is a central hub of primary plant metabolism, serving biosynthesis, catabolism and energy conversion. Its integrative role in the cellular metabolic network requires unique flexibility of TCA cycle flux in plants, and several different flux modes, both cyclic and non-cyclic, have been reported depending on the physiological circumstances (Sweetlove *et al.*, 2010). In heterotrophic Arabidopsis cells a cyclic flux mode can be anticipated. The ten enzymatic steps of the TCA cycle (including pyruvate dehydrogenase and NAD-malic enzyme) are represented by 176 358 protein copies per mitochondrion, corresponding to 12.7% of mitochondrial protein content (Table S1). Assuming that the matrix volume takes up 50% of the total mitochondrial volume (Møller, 2016), and estimating the protein volume from available protein crystal structures of non-plant species (Dataset S2, worksheet #9, TCA cycle proteins are well-conserved), the TCA cycle enzymes occupy 16.8% of the matrix volume (0.0225 μm^3 out of 0.134 μm^3, Figure 3; Dataset S2, worksheet #9). This equals 80.5% of the protein volume of the matrix (assuming similar average density of the proteins as of the mitochondrion overall and similar weight contribution of proteins to matrix as to whole mitochondrion). The two large multi-enzyme complexes PDC (*Mr* ~10^7) and 2-oxoglutarate dehydrogenase (OGDC; *Mr* ~4×10^6) alone account for 11.2% of the total matrix volume (10.2% and 1.0%, respectively, corresponding to 49.0% and 4.7% of matrix protein volume) (Figure 3; Dataset S2, worksheet #9). The total number of PDC and OGDC is as small as 222 and 181, respectively, as multiple functional enzymes are organised in these megacomplexes (Zhou *et al.*, 2001) (active units E1, E2 and E3 in 5:5:2 stoichiometry; PDC: 14 204 protein copies, OGDC: 12 998

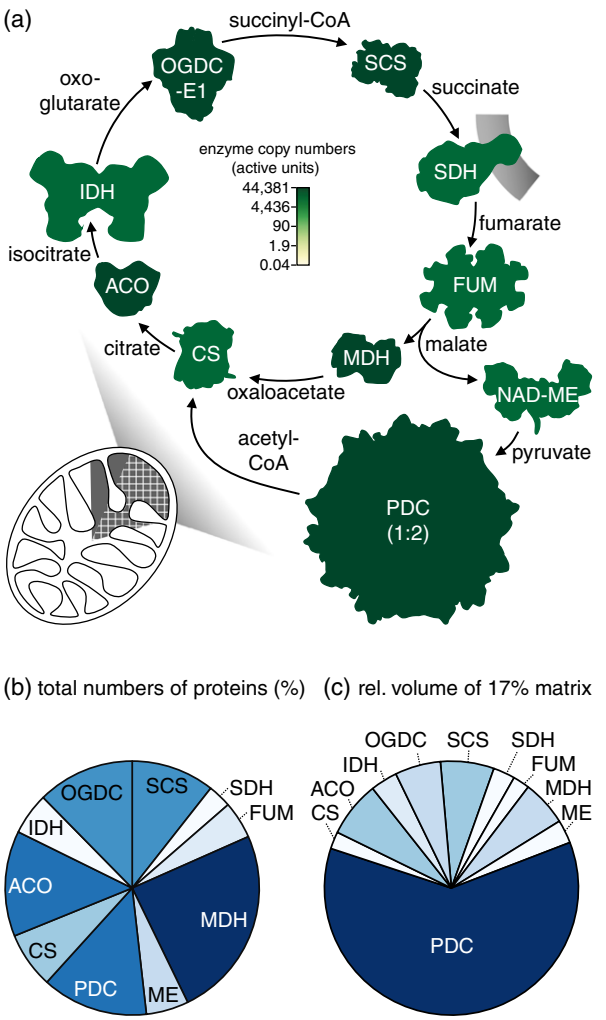

Figure 3. TCA cycle enzymes.
(a) Matrix volume occupied by all matrix proteins shaded in grey (20.8%), contribution of TCA cycle enzymes grid patterned (16.8%). Enzyme structures show physiologically relevant oligomerisation (active enzymes): citrate synthase (CS) as dimer, aconitase (ACO) as monomer, isocitrate dehydrogenase (IDH) as hetero-octamer of four outer catalytic and four inner regulatory subunits, pyruvate dehydrogenase complex (PDC) scaled down in displayed size by half (1:2) compared to all other enzymes and the 2-oxoglutarate dehydrogenase (OGDC)-E1 subunit as homodimer, succinyl-CoA-synthase (SCS) as heterotetramer (two α- and two β-subunits), succinate dehydrogenase (SDH) as monomer, fumarase (FUM) as tetramer, malate dehydrogenase (MDH) as homodimer, NAD-malic enzyme (NAD-ME) as homodimer.
Pie charts show (b) the proportion of enzymes (active units in %) to the total numbers of TCA cycle proteins (physiologically active units: 105 135) and (c) the contribution of each TCA enzyme relative to the TCA enzyme-occupied matrix space (%).

protein copies). Aconitase (ACO) and malate dehydrogenase (MDH) are both comparatively small proteins, but high in abundance (14 121 and 25 684 copies), contributing 1.2% and 1.0% of the total matrix volume, each. Succinate dehydrogenase (SDH) is the only integral membrane protein linking the TCA cycle with the respiratory electron transport chain. Its matrix-exposed part accounts for 0.5% total matrix volume, while it makes up 0.8% of the IMM area (assuming an IMM:OMM ratio of 3:1, Schwerzmann *et al.*, 1986). SDH makes the smallest contribution to the total number of TCA cycle enzymes (3156 SDH complex monomers). The large contribution of TCA cycle enzymes to fill the crowded matrix volume makes substrate diffusion between enzymes extremely efficient and the discrimination of functional protein–protein interactions for metabolon formation from more random interactions particularly challenging (Zhang *et al.*, 2017).

A mitochondrion has the capacity to metabolize its own mass worth in malate within 1 h. Different from mammals where pyruvate is the primary TCA cycle substrate, the main substrate can vary between metabolic states in plants and malate plays a particularly prominent role (Sweetlove *et al.*, 2010). Malate is metabolized through two different reactions catalyzed by NAD-malic enzyme (NAD-ME) and malate dehydrogenase (MDH) (Figure 3) (Maurino and Engqvist, 2015). NAD-ME1 and NAD-ME2 associate to form active homo- and heterodimers to metabolize malate to pyruvate. A single mitochondrion contains similar amounts of NAD-ME1 (2632 copies) and NAD-ME2 (3061 copies) (Dataset S1, worksheet #1 and S2, worksheet #10). In a heterotrophic organ, such as roots, the total NAD-ME activity is composed of 8% NAD-ME1 homodimers, 32% NAD-ME2 homodimers, and 60% heterodimers (Tronconi *et al.*, 2008). Applying those contributions to the single mitochondrion, there are 155 NAD-ME1 homodimers (310 NAD-ME1 copies), and 2322 heterodimers (2322 NAD-ME1 copies). Analogously, 1065 copies of NAD-ME2 are present in 532 homodimers, and 1996 copies contribute to 1996 heterodimers. The independent consideration of NAD-ME1 and 2 result in similar copy numbers involved in heterodimers (2322 versus 1996) in line with their 1:1 stoichiometry in the complex. Based on the enzymatic turnover numbers determined *in vitro* for the three different dimer types (Tronconi *et al.*, 2010), a single mitochondrion has a total NAD-ME capacity to metabolize 224 852 malate molecules per second (Dataset S2, worksheet #10).

An analogous estimation for mitochondrial MDH (13 190 copies of MDH1; 10 826 copies of MDH2; Dataset S2, worksheet #10 and S3, worksheet #4) suggests that total MDH capacity is at 183 625 malate molecules per second (Dataset S2, worksheet #10). This estimation is based on the *in vitro* turnover numbers for the reverse reaction of OAA to malate and the consideration that MDH1 and MDH2 have 80-fold and 34-fold higher maximal activity for OAA than for malate as substrate (Hüdig *et al.*, 2015). The capacities of NAD-ME and MDH for malate turnover appear to be similar and add up to 408 477 molecules of malate per second. This equals a mass of 54.8 MDa per second adding up to the mass of the entire single mitochondrion over the course of 59 min (Dataset S2, worksheet #10). This remarkable capacity appears highly above of what is typically required for malate oxidation *in vivo*, but is generally consistent with previous indications that MDH (but not NAD-ME) is present at > 100-fold excess (Hagedorn *et al.*, 2004). Carbon flux through MDH and NAD-ME will certainly be constrained by several influences, including malate uptake into the matrix, efficient product removal, and recycling of NAD^+, but the high combined capacity of MDH and NAD-ME emphasizes the significance of malate metabolism in plant mitochondria.

The copy numbers of glycine decarboxylase and serine hydroxymethyltransferase proteins mirror metabolic demands of the cell. The glycine decarboxylase complex (GDC) acts together with the serine hydroxymethyltransferase (SHMT) to convert glycine to serine, which is an essential step in the photorespiratory cycle (Bauwe *et al.*, 2010; Peterhänsel *et al.*, 2010) and in N^5,N^{10}-methylene tetrahydrofolate provision for one-carbon metabolism (Engel *et al.*, 2007; Maurino and Peterhänsel, 2010).

The GDC is a multi-enzyme system of four loosely associated P-, H-, T- and L-proteins (Bauwe and Kolukisaoglu, 2003; Peterhänsel *et al.*, 2010). The four proteins are present in unequal molar amounts, but the exact stoichiometric composition of the Arabidopsis complex is not yet established. The GDC components in the heterotrophic Arabidopsis cell suspension culture mitochondria, in which photorespiration is not active, accounts for only a small fraction (0.18%) of the mitochondrial proteome mass (Dataset S2, worksheet #11). This is consistent with the idea that the abundance of the GDC proteins positively correlates with the photosynthetic activity (Bourguignon *et al.*, 1993; Mouillon *et al.*, 1999). GDC contributes up to 32% of the total matrix protein in photosynthetically active pea leaves (Oliver *et al.*, 1990). In the heterotrophic cell suspension culture mitochondria only 0.57% of the total matrix space is occupied by GDC (Dataset S2, worksheet #11). We found 807 copies of GDC-P, 2503 copies of GDC-H, 2577 copies of GDC-T, 14 990 copies of GDC-L (MTLPD1: 4876; MTLPD2: 10 114) per mitochondrion (Datasheet S1, worksheet #1; Dataset S3, worksheet #5). The excess of the L-proteins detected may be explained by the additional participation as E3 subunits of the pyruvate and 2-oxoglutarate dehydrogenase complexes assuming that both L-proteins are shared between GDC, PDC, OGDC and

branched-chain α-ketoacid dehydrogenase (BCKDH) (Bourguignon *et al.*, 1992, 1996; Lutziger and Oliver, 2001). The shared contribution of the L-proteins to the former three dehydrogenase complexes was considered in the calculations (Dataset S2, worksheets #9 and #11). Assuming that the turnover rates of the P-proteins from Arabidopsis are similarly low as those of *Synechocystis* (Hasse *et al.*, 2007), the GDC has the capability of converting only 115 molecules glycine per second in the cell suspension culture single mitochondrion (Dataset S2, worksheet #11).

Serine hydroxymethyltransferase (SHMT) is present at higher copy numbers than GDC, which is mainly due to SHMT2 (3885 copies; SHMT1: 38 copies). The low representation of SHMT1 can be explained by its involvement in photorespiration, which is not active in the heterotrophic mitochondrion (Somerville and Ogren, 1981; Engel *et al.*, 2011), while SHMT2 is typically not present in photosynthetically active cells (McClung *et al.*, 2000; Bauwe and Kolukisaoglu, 2003). Assuming that the turnover numbers of SHMT1 and 2 are similar to that of the plastidial isoform (Zhang *et al.*, 2010), the heterotrophic mitochondrion has the capability of producing 61 989 molecules of serine and tetrahydrofolate per second (Dataset S2, worksheet #11), indicating active one-carbon metabolism.

High copy numbers reflect the essential functions of mitochondrial amino acid catabolism enzymes. Beyond glycine catabolism, mitochondria are a major site of amino acid degradation. The different catabolic pathways give rise to several intermediates of mitochondrial carbon metabolism (Hildebrandt *et al.*, 2015). The proteome here generated includes almost all presently known mitochondrial steps of the amino acid catabolic pathways, i.e. the enzymes catalyzing the degradation of branched-chain amino acids, Pro and Arg, Cys, as well as Ser/Gly metabolism (Dataset S3, worksheet #6).

The degradation pathways of most amino acids require transfer of the amino group to 2-oxoglutarate catalyzed by a diverse set of aminotransferases followed by oxidative deamination of Glu by glutamate dehydrogenase (GDH) (Hildebrandt *et al.*, 2015). Consistently, GDH2 is the most abundant amino acid metabolic enzyme and with 12 933 copies per mitochondrion it is the twelfth most abundant protein of the mitochondrion overall. GDH1 is present at 4269 copies further boosting the enzymatic capacity of GDH. Several aminotransferases operating upstream of GDH are also present at high copy numbers, the most abundant being GABA transaminase (5418 copies), aspartate aminotransferase 1 (5347 copies) and alanine aminotransferase 1 (4728 copies).

The prominence of mitochondrial Cys metabolism, as a hub of several downstream pathways is emphasized by high copy numbers of mitochondrial O-acetylserine (thiol) lyase (OASC; 3571 copies) required for Cys synthesis and regulation (Wirtz *et al.*, 2012), the Cys desulfurase NifS (4265 copies) involved in the synthesis of iron-sulfur clusters and of β-cyanoalanine synthase (CAS; 12 218 copies). CAS catalyzes the substitution of the Cys sulfhydryl group with cyanide to produce the β-cyanoalanine and H_2S (Hatzfeld *et al.*, 2000). The main physiological function of CAS is thought to be the detoxification of cyanide produced during ethylene synthesis to protect cytochrome *c* oxidase from irreversible inhibition. The 12 218 copies of CAS exceed those of complex IV markedly (1916 copies, see above). Considering the fact that the flux of cyanide production in the cell is very low in comparison to respiratory flux, a very high copy number of CAS in the matrix, i.e. in direct vicinity to the active site of cytochrome *c* oxidase, reflects the potentially detrimental effect of cyanide inhibition and the importance of the activity of the cyanide-sensitive pathway of respiration.

Antioxidant enzyme capacity exceeds mitochondrial ROS production by far. The generation of reactive oxygen species (ROS) in mitochondria requires a tight balance between ROS scavenging, ROS signalling functions and redox regulation of mitochondrial metabolism. Molecular oxygen is the terminal electron acceptor of the ETC where it accepts four electrons and is fully reduced to water. In addition, and at much lower rate, single electrons can be transferred to molecular oxygen at specific sites of the ETC, which gives rise to superoxide. The rate of superoxide production can vary considerably depending on the overall respiratory activity and substrate availability in the mitochondrion (Møller, 2001; Murphy, 2009). In isolated soybean mitochondria (state II), superoxide production of up to 1.3 nmol min^{-1} mg^{-1} protein was observed when mitochondria were fed with respiratory substrates for complex I+II. Hence, it was estimated that up to 5.9% of the respiratory electron flow ends up in superoxide production (Puntarulo *et al.*, 1988). This number is likely to be smaller *in vivo*, but provides a useful upper limit. In mitochondria isolated from Arabidopsis seedlings and cell suspension culture, state III respiratory rates typically reach 200 nmol O_2 min^{-1} mg^{-1} protein (Eubel *et al.*, 2007; Wagner *et al.*, 2015), which would result in a superoxide production of up to 11.8 nmol O_2^- min^{-1} mg^{-1} protein. Superoxide itself is unstable and dismutates into hydrogen peroxide and molecular oxygen with a rate constant of 5×10^5 M^{-1} sec^{-1}. Yet, superoxide also inactivates Fe/S cluster-containing proteins, such as aconitase, with rate constants of 10^6 to 10^7 M^{-1} sec^{-1} (Halliwell and Gutteridge, 2015). Manganese superoxide dismutase (MnSOD) competes with those reactions in the mitochondrial matrix, catalysing rapid superoxide dismutation. MnSOD (MSD1) was detected among the top 30 most abundant mitochondrial proteins (11 223 copies per mitochondrion) with a similar abundance to aconitase 3 (9898 protein copies). As

MnSODs reach turnover numbers (k_{cat}) of 40 000 sec^{-1} and k_{cat}/K_m of 8×10^8 M^{-1} sec^{-1} (Hsu *et al.*, 1996), the SOD capacity in a single mitochondrion is sufficient to detoxify 448 932 392 molecules of superoxide per second. This rate exceeds even generous estimates of superoxide generation by a factor of 39 000-fold (Dataset S2, worksheet #12). Potentially, the large amount of MnSOD copies present can be explained by increasing the probability for each superoxide molecule generated to be detoxified by MnSOD before encountering a Fe/S cluster-containing enzyme. The enormous SOD capacity in the mitochondrial matrix matches the observation that MnSOD activity is not rate-limiting in ROS detoxification under stress (Kliebenstein *et al.*, 1998).

As superoxide dismutation leads to O_2 and hydrogen peroxide (H_2O_2) formation, it was estimated that 0.9–1.5% of consumed O_2 is converted to H_2O_2 (Puntarulo *et al.*, 1988), which would result in up to3 nmol H_2O_2 min^{-1} mg^{-1} $protein^{-1}$ at typical state III respiratory rates. Matrix peroxidases reduce H_2O_2 to water using either glutathione, ascorbate or the thioredoxin (Trx) system as electron donors. The most abundant peroxidase in the mitochondrion is peroxiredoxin II F (PrxII F) at 5787 copies, i.e. half the copy number of MnSOD. While that ratio matches the stoichiometry of H_2O_2 molecules to be detoxified per superoxide molecule (1:2), PrxII F has a much lower turnover number than MnSOD (0.67 sec^{-1} versus 40 000 sec^{-1}) (Finkemeier *et al.*, 2005) meaning that only 3877 H_2O_2 molecules can be reduced to water in a single mitochondrion per second. Induction of PrxII F protein abundance by more than 3-fold was observed in response to oxidative stress treatments (Sweetlove *et al.*, 2002), indicating that baseline PrxII F capacity can become limiting and needs to be increased under stress. Alternatively, the physiological role of PrxII F may be the oxidation of target thiols in the mitochondrial matrix, similar to the function of plastidic 2-Cys Prx (Pérez-Ruiz *et al.*, 2017; Vaseghi *et al.*, 2018). After oxidation, PrxII F has to be regenerated by glutathione or the thioredoxin (Trx) system (Finkemeier *et al.*, 2005). Both Trx-o1 (837 copies) and -o2 (20 copies) were detected in the mitochondrial proteome, as well as the mitochondrial NADPH-dependent thioredoxin reductases a (Ntra; 913 copies) and b (Ntrb; 342 copies), both of which have been found dual-targeted to the cytosol and the mitochondrial matrix (Reichheld *et al.*, 2007). A high capacity for superoxide removal and a low capacity for H_2O_2 removal mirror the different physiological roles of the two reactive species. While superoxide will be quenched efficiently in the matrix, H_2O_2 fluctuations in matrix H_2O_2 remain plausible, as well as diffusion out of the matrix, consistent with the likely roles of H_2O_2 in intracellular signalling (Huang *et al.*, 2016).

However, there are additional peroxidases with much higher turnover numbers for H_2O_2 in the mitochondrion (Dataset S3, worksheet #7). The dual-localized stromal ascorbate peroxidase (sAPX) (Chew *et al.*, 2003) was detected at 1708 copies. Assuming that all detected protein comes from the mitochondrion (rather than from plastid contaminations) and a turnover number for H_2O_2 of 1800 sec^{-1} as for the tobacco sAPX (Kitajima *et al.*, 2008), the capacity of sAPX in a single mitochondrion is 3.07 Mio molecules of H_2O_2 per second. Although this generous estimate equals less than 1% of the MnSOD capacity, it mirrors a dominant role to sAPX in quenching a major share of the H_2O_2 flux in the matrix.

Mitochondria host co-factor biogenesis including iron-sulfur clusters, biotin, lipoic acid, tetrahydrofolate and potentially the last step of heme synthesis. A key function of mitochondria is the biogenesis of essential cofactors including iron-sulfur (Fe/S) clusters, biotin, lipoic acid and tetrahydrofolate. Proteins involved in the Fe/S assembly pathway are the most abundant of this category (above the average copy number of 474 copies) whereas the enzymes involved in biotin, lipoic acid and tetrahydrofolate biogenesis are detected at much lower copy numbers (21–347 copies; Figure 4; Dataset S3, worksheet #8). Interestingly, some enzymes (NSF1, BIO2 and HPPK/DHPS2) are present in excess compared to the others involved in the same pathway. This may reflect differing enzymatic capacities per protein, protein-specific inactivation through oxidative damage and/or different roles in the control of metabolic flux through the respective pathway. Proteins involved in the delivery of the cofactors to apoenzymes are less abundant than biosynthetic enzymes (Figure 4). Electrons provided by a ferredoxin reductase/ferredoxin (FDR/MFDX) system are required in three of these biosynthetic pathways. The two isoforms of MFDX detected show very differing copy numbers (MFDX1: 73 and MFDX2: 494). Based on the respective abundances of MFDX isoforms and biosynthetic enzymes, it is tempting to speculate that MFDX1 plays a role in biotin and lipoic acid biosynthesis, whereas MFDX2 is involved in Fe/S clusters biogenesis.

In plants, the heme synthesis pathway is located in the plastids (Tanaka and Tanaka, 2007), but its last step, i.e. the chelation of iron, was proposed to be also performed in mitochondria (Chow *et al.*, 1997, 1998; Hey *et al.*, 2016), however this has been disputed (Lister *et al.*, 2001; Masuda *et al.*, 2003; Woodson *et al.*, 2011). Several proteins involved in heme biosynthesis were identified in our analysis (Dataset S3, worksheet #8), albeit at low copy numbers (<80 copies), indicating etioplast contamination of our mitochondria isolations. Remarkably, the ferrochelatase (FC1) shows a copy number (78 copies) higher than the remaining proteins of the pathway (less than 26 copies, excluding the dual-targeted glutamyl-tRNA synthase), which may support the hypothesis that the last step of heme biosynthesis is actually present in plant mitochondria.

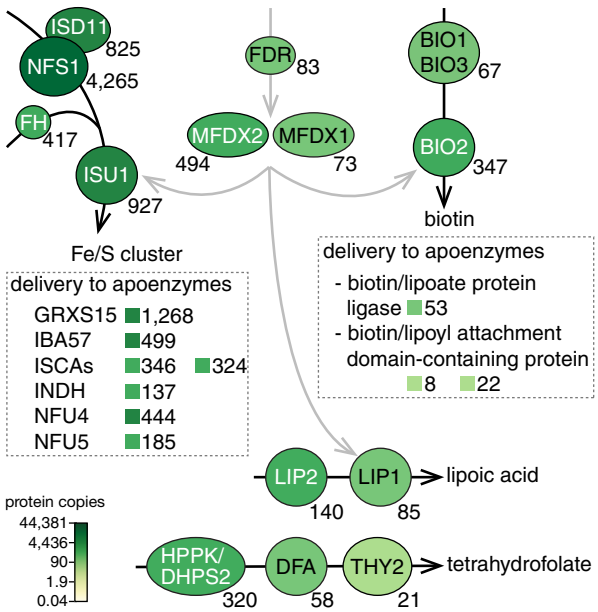

Figure 4. Cofactor biogenesis pathways.
Simplified representation of the mitochondrial steps of the biosynthesis pathways of Fe/S clusters, biotin, lipoic acid and tetrahydrofolate. Each pathway is represented with black arrows. The biosynthetic enzymes are represented as circles. The final product of the pathway is indicated in black. No substrates or intermediates are shown. The grey arrows represent electron transfers. Proteins involved in the delivery of the cofactor to the apoenzymes are indicated in dashed boxes together with their copy numbers. Cysteine desulfurase (NFS1); NFS1 interacting protein (ISD11); frataxin (FH); iron-sulfur cluster assembly protein 1 (ISU1); glutaredoxin S15 (GRXS15); iron-sulfur cluster assembly factor for biotin synthase- and aconitase-like mitochondrial proteins, with a mass of 57 kDa (IBA57); iron-sulfur cluster A-type carrier (ISCA); homologous to iron-sulfur protein required for NADH dehydrogenase (INDH); NifU-like protein (NFU); ferredoxin reductase (FDR); mitochondrial ferredoxin (MFDX); biotin synthase (BIO); lipoic acid synthase (LIP); bifunctional hydroxymethyl-dihydropterin-pyrophosphokinase and dihydropteroate synthase (HPPK/DHPS); folylpolyglutamate synthase (DFA); thymidylate synthase (THY).

Writers and erasers of several reversible protein modifications are present at low copy number in plant mitochondria. Reversible post-translational modifications play an important role for transient regulations of mitochondrial activities (Hartl and Finkemeier, 2012). Protein modifications derived from the metabolic cofactors ATP, *S*-adenosylmethionine, and acetyl-CoA as well as other acyl-CoA metabolites are present at a high abundance in mitochondria (Finkemeier and Schwarzländer, 2018). Although inventories of several of these protein modifications were reported for Arabidopsis mitochondria (Ito *et al.*, 2009; König *et al.*, 2014a; van Wijk *et al.*, 2014; Hosp *et al.*, 2017), most of the writers and erasers of these modifications are unknown.

The light-dependent inactivation of the pyruvate dehydrogenase E1 subunit by phosphorylation via pyruvate dehydrogenase kinase (PDK) represents an important example of a known writer (Mooney *et al.*, 2000). We identified 120 PDK copies and 8944 copies of its substrate, the catalytic pyruvate dehydrogenase (PDH) E1 β-subunit. Assuming the mammalian PDK kinase activity of 70 nmol min^{-1} mg^{-1} of PDH-E1 (Bowker-Kinley and Popov, 1999), the analogous phosphorylation of one site in all PDH-E1 copies (corresponding to 1.49×10^{-11} nmol) would take 26 min (Dataset S2, worksheet #13). Notably, this time range is similar to the time that it takes to dark-adapt photosynthetic tissues (20–30 min) (Murchie and Lawson, 2013).

While the PDK was already identified nearly 20 years ago, the identity of the pyruvate dehydrogenase phosphatase remains unknown. A protein phosphatase 2C family protein was identified in potato mitochondria as a candidate (Salvato *et al.*, 2014), and the Arabidopsis homologue is present at eight copies per mitochondrion (Dataset S3, worksheet #9). Similar (low) copy numbers of both the kinase and the phosphatase per mitochondrion may be regarded as further evidence for their function as a regulatory couple. Another phosphatase, SLP2, which is present in the IMS, and involved in the regulation of seed germination (Uhrig *et al.*, 2017), was detected at comparably low copy number (296 copies).

Similar to the protein phosphatases as erasers, two different protein lysine deacetylases, Sirtuin 2 (SRT2) and HDA14, were recently identified to reside in Arabidopsis mitochondria (Hartl and Finkemeier, 2012; König *et al.*, 2014b). SRT2, which functions as a lysine deacetylase of proteins, such as of the ATP/ADP carrier, at the matrix side of the IMM, was detected in this dataset with only 23 copies. It appears that SRT2 is of higher abundance in mitochondria of green Arabidopsis seedlings where around 323 copies per mitochondrion were found (König *et al.*, 2014b). The absence of SRT2 in isolated Arabidopsis mitochondria led to increased ATP export rates as mediated by increased activity of the ATP/ADP-carrier AAC1, suggesting a direct role of acetylation in modulating cellular ATP provision by the mitochondrion. Since the kinetic properties of sirtuins are highly dependent on their specific protein substrates, it is not possible to estimate catalytic capacities for the deacetylation rates of AAC1. No candidate acetyltransferase protein was identified in this dataset, which might either indicate that the acetyltransferase is of even lower abundance and below detection limit or that acetylation solely occurs non-enzymatically in the matrix, driven by alkaline conditions (König *et al.*, 2014a). All modifying enzymes detected in this study were of particular low abundance, which fits their predicted regulatory functions.

Substoichiometric amounts of mitochondrial DNA are reflected by low copy numbers of DNA-binding proteins. The plant mitochondrial genome is maintained in the organelles separately from the nuclear genome.

Proteome profiling identified the single-stranded DNA-binding proteins Whirly2 (WHY2), Organellar DNA-binding protein 1 (ODB1), Single-stranded DNA-binding proteins 1 and 2 (SSB1, SSB2), RecA homolog 2 (RECA2) and the enzyme DNA gyrase as the most abundant DNA-binding proteins in Arabidopsis mitochondria (Figure 5). The most abundant of these, WHY2, is present at 974 copies, corresponding to 41 24-mers (oligomeric status according to Cappadocia *et al.* (2012)). Arabidopsis mitochondria contain only one full genome per approximately three organelles, meaning that 122 kbp of mitochondrial DNA are present per mitochondrion on average (Preuten *et al.*, 2010). Based on these numbers and assuming that all protein copies of WHY2 are bound to DNA *in vivo*, WHY2 is present at three 24-mers per 10^4 bases. By comparison, the major DNA-binding protein of human mitochondria, mitochondrial Transcription factor A (TFAM), is bound to DNA at 600 molecules per 10^4 base pairs (Kukat *et al.*, 2011). Assuming that each WHY2 protomer within a 24-mer binds 9 nt of ssDNA (Cappadocia *et al.*, 2012), SSBs bind 30 or 60 nt per tetramer (Qian and Johnson, 2017), and RECA2 binds 3 nt per protomer of the RECA2 filament (Cox, 2007), these abundant proteins will cover between 7 and 11% of the mitochondrial genome. Another 3% can be estimated to be bound by ODB1 and the OSB family (Dataset S2, worksheet #14). Based on these numbers, (i) at least 80% of the Arabidopsis mitochondrial genome are "naked", i.e. not covered by protein, and (ii) 10–15% of the mitochondrial genome are kept in a single-stranded configuration by ssDNA-binding proteins. These estimates are based on the assumption that all proteomically detected DNA-binding proteins are bound to DNA *in vivo*. We might therefore underestimate the proportion of naked DNA and overestimate the proportion of ssDNA. An earlier study reported about 7% of ssDNA for mitochondria of *Chenopodium album* (Backert *et al.*, 1997).

Two DNA-binding proteins are present at extremely low copy numbers (Organellar single-stranded DNA binding protein 1 [OSB1] and MutS protein homologue [MSH1]), and a third, RECA3, was not detected. All three proteins are critical for mtDNA maintenance since their knockout causes dramatic mtDNA lesions that accumulate over generations (Zaegel *et al.*, 2006; Shedge *et al.*, 2007). Our proteomic data indicate only four copies of OSB1 and two copies of MSH1 per mitochondrion. Assuming that MSH1 functions as a dimer (Gualberto and Newton, 2017), only one functional unit of this protein is found per mitochondrion. This possibly reflects the low expression of these proteins in any tissue other than gametophytes. The DNA gyrase complex (about 400 copies) is by far the most abundant enzyme acting on mitochondrial DNA, about 100-fold more abundant than each of the DNA polymerases POL1A (five copies) and POL1B (two copies). This implies that only a minor portion of the mitochondrial DNA gyrase pool is required to relax DNA during replication. Surprisingly the RNA polymerase RPOTm, which has been considered the major RNA polymerase in dicot mitochondria owing to its loss being intolerable in Arabidopsis (Kühn *et al.*, 2009), is present at only five copies per mitochondrion. Thus, the nonessential RPOTmp, present at 31 copies per mitochondrion, may be the major RNA polymerase in dicot mitochondria. Assuming that plant mitochondrial RNA

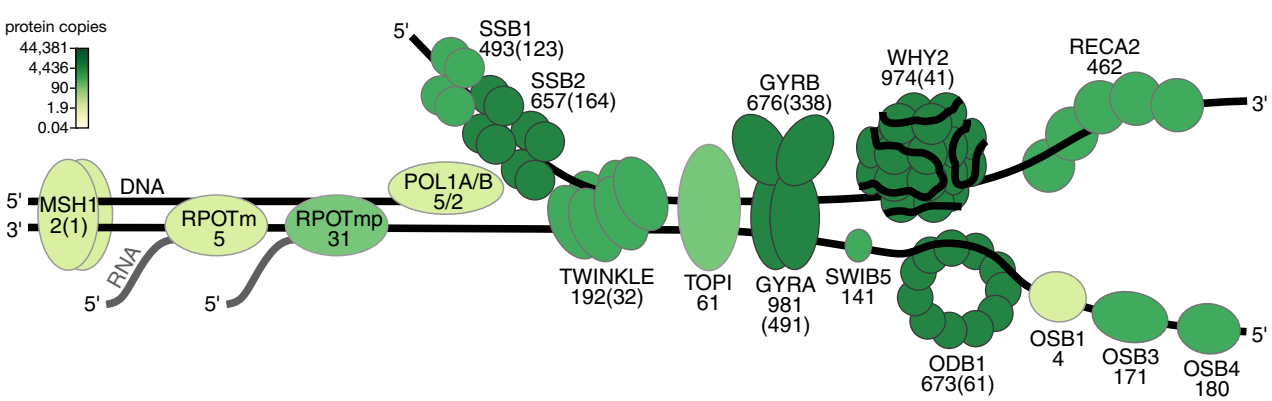

Figure 5. Proteins associated with the mitochondrial genome.
DNA-binding proteins detected are represented as binding to single-stranded or double-stranded DNA (based on findings recently reviewed by Gualberto and Kühn, 2014; Gualberto and Newton, 2017). The DNA polymerases 1A (POL1A) and 1B (POL1B) are summarized by a single symbol. For proteins known or assumed to be present in homo- or hetero-oligomers the inferred number of complexes is shown in brackets. For DNA gyrase composed of two DNA gyrase A (GYRA) and two DNA gyrase B (GYRB) subunits each, the subunits are of similar abundance (981 versus 676), which allows estimating about 400 enzyme complexes per mitochondrion. RecA homolog 2 (RECA2); MutS homolog 1 (MSH1); organellar DNA-binding protein 1 (ODB1); organellar single-stranded DNA-binding protein (OSB1, OSB3, OSB4); T3/T7 bacteriophage-type RNA polymerase, mitochondrial (RPOTm); T3/T7 bacteriophage-type RNA polymerase, mitochondrial/plastidial (RPOTmp); mitochondrial single-stranded DNA-binding protein (SSB1, SSB2); SWI/SNF protein complex B protein 5 (SWIB5); Type-IA DNA topoisomerase (TOPI), twinkle-like DNA primase-helicase (TWINKLE); Whirly 2 (WHY2). Not included in the figure: homolog of bacterial RecG (RECG1, four copies), DNA repair protein RadA-like protein (RADA, 34 copies); protein related to *Escherichia coli* RuvC, involved in homologous recombination (Gualberto and Newton, 2017) (eight copies); DNA Ligase I (47 copies).

polymerases elongate at a rate of 50 nucleotides per second, which is the average rate reported for bacterial and nuclear enzymes (Vogel and Jensen, 1994; Bubulya and Spector, 2004; Pérez-Ortín *et al.*, 2007), RPOTm and RPOTmp together can transcribe 108 kb of DNA per minute. This is in the range of the DNA present per mitochondrion (see above), and about three times the transcribed part of that DNA, according to transcriptome data indicating that about 30% of the Arabidopsis mitochondrial genome are transcribed.

Most RNA-processing and RNA-editing PPR proteins are present at low copy numbers. The RNA-binding and -processing PPR proteins constitute one of the largest gene families in the nuclear genome of *A. thaliana* (496 genes, Cheng *et al.*, 2016). The majority, 278 members, are mitochondrial localized as identified by SUBAcon (Hooper *et al.*, 2014). Out of these, 107 were detected here (Dataset S3, worksheet #11). It is reasonable to interpret the relatively low detection coverage as a reflection of the generally low copy number of the PPR proteins per mitochondrion. This is supported by the observation that more than 60% of the identified PPR proteins were represented by less than 20 copies per mitochondrion (Figure 6; Dataset S3, worksheet #11). Although PPR proteins contributed only 1.4% of the complete proteome mass, they represented 4.7% of the identified protein species.

Structurally, PPR proteins are classified into two different subgroups, P- and PLS-type. Most PLS-type PPR proteins act as specific C-to-U editing factors (Barkan and Small, 2014), many of them with a C-terminal DYW-domain as cytidine deaminase (Oldenkott *et al.*, 2019). They are particularly lowly abundant with protein copies ranging from 0.83 (i.e. substoichiometric) to 34. Notably, the PLS-type protein DYW2 contrasted this tendency and was present at 351 copies per mitochondrion. DYW2 lacks an extended upstream PPR array and is, in contrast to most other PLS-type PPR proteins, involved in editing of many sites providing the DYW domain *in trans* (Andrés-Colás *et al.*, 2017; Guillaumot *et al.*, 2017). The comparatively high copy numbers suggest that DYW2 constitutes a general component of the editosome in Arabidopsis. In support of that, the copy numbers of most other editing proteins like the Multiple Organellar RNA-editing Factors (MORFs, Takenaka *et al.*, 2012), the Organelle RNA Recognition Motif-containing proteins (ORRMs) or the Organellar Zinc finger proteins (OZs, Sun *et al.*, 2016), which support editing at many sites, are comparable to those of DYW2 or even higher (Figure 6; Dataset S3, worksheet #11).

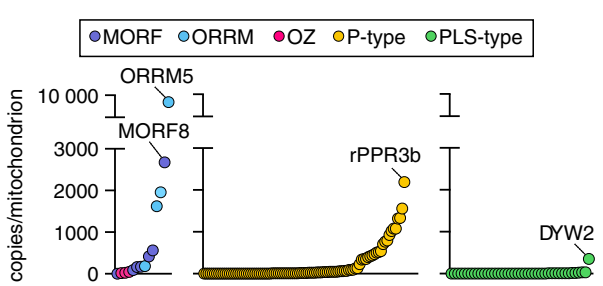

Figure 6. Copy numbers of RNA-processing and RNA-editing proteins.
The identified proteins of three different groups involved in RNA-processing and RNA-editing in particular P-type, PLS-type pentatricopeptide repeat (PPR) proteins and additional RNA-editing proteins (multiple organellar RNA-editing factors [MORFs, Takenaka *et al.*, 2012]/organelle RNA recognition motif-containing proteins [ORRMs]/organellar zinc finger proteins [OZs, Sun *et al.*, 2016]) are plotted with increasing abundance (copy number/single mitochondrion). Highlighted are the most abundant proteins of each group: P-type PPR protein rPPR3b with 2189 copies, PLS-type PPR protein DYW2 with 351 copies, ORRM5 with 7857 copies and MORF8 with 2676 copies per mitochondrion.

Of the P-type subgroup, we identified 58% of the mitochondrial-predicted proteins (95 out of 165) with copy numbers ranging from 0.6 to 2189. In contrast to most PPR proteins, all of the currently characterized and relatively highly abundant P-type PPR proteins seem not to recognize single specific RNA targets but act via less specific protein–protein or protein–rRNA interactions (Waltz *et al.*, 2019). Among them are the 10 recently identified ribosome-associated PPR proteins (Rugen *et al.*, 2019a,b; Waltz *et al.*, 2019), including two of the three most abundant PPR proteins rPPR3b (2189 copies) and PPR336 (1335 copies), and NUWA (1077 copies), which interacts with DYW2 as part of the RNA editosome (Andrés-Colás *et al.*, 2017; Guillaumot *et al.*, 2017).

However, most P- and PLS-type PPR proteins act on particular RNA targets only and are fundamental for the efficient processing of specific mitochondrial transcripts, e.g. by RNA-editing, 5′ and 3′ processing or intron splicing (Bentolila *et al.*, 2013; Barkan and Small, 2014; Brown *et al.*, 2014). Interestingly, the copy numbers for these proteins were generally very low or even substoichiometric to the mitochondrial population. This was also the case for non-PPR RNA-processing factors with specific targets like the maturases or the PORR-protein WTF9 (Brown *et al.*, 2014; Dataset S3, worksheet #11). We identified only one (nMAT2, 34 copies) of the five maturases, required for splicing of individual group II introns. The high abundance of the DEAD-box protein PMH2 (1322 copies) can be explained by its general role in RNA stabilisation (Köhler *et al.*, 2010). Low numbers of RNA-processing factors indicate that continuous mitochondrial fusion and fission may be crucial to ensure proper function of the gene products that require post-transcriptional modification.

The copy numbers of proteins involved in mitochondrial dynamics indicate frequent, but heterogenic, fission events. The balance between mitochondrial fusion and fission events controls mitochondrial genome distribution, mitochondrial size, shape and number within a cell, and mitochondrial segregation between the daughter cells

during cell division (Arimura *et al.*, 2004b; Sheahan *et al.*, 2004, 2005; Logan and Paszkiewicz, 2017). While the genetic components of the fusion machinery are unknown in plants, several proteins involved in fission have been identified (Arimura *et al.*, 2004b; Logan and Paszkiewicz, 2017). All established components of the fission machinery were found in the proteomic dataset (Figure 7; Dataset S2, worksheet #12), with the exception of Fission1b (FIS1B) and Elongated mitochondria 2 (ELM2), whose contribution in the mitochondrial division seems to be marginal (Arimura *et al.*, 2017), and FRIENDLY, which is a cytosolic protein only transiently associated with the mitochondria (El Zawily *et al.*, 2014). A total of 2108 copies of proteins involved in mitochondrial fission were identified per mitochondrion, with Elongated mitochondria 1 (ELM1), and Peroxisomal and mitochondrial division factors (PMD2 and PMD1) being the most abundant (286, 1300 and 402 copies, respectively). ELM1 is a plant-specific adapter protein directing dynamin-related proteins (DRP3) to fission sites while putatively interacting with the outer mitochondrial membrane tail-anchored Fission1 (FIS1) proteins (Arimura *et al.*, 2008; Scott and Logan, 2011). However, DRP3A localisation to mitochondria occurred independent of ELM1 in cold-induced mitochondrial fission (Arimura *et al.*, 2017). Here, FIS1A (53 copies) was detected at a similar copy number to that of the sum of the two Dynamin-related protein 3 (DRP3A, B) isoforms (67 copies), while the ELM1 copy number was 4 times higher (286 copies). The reason for the excess of ELM1 is unclear and suggests FIS-independent functions or that yet unknown, plant-specific membrane proteins are involved in the recruitment of ELM1 to the outer mitochondrial membrane.

During fission DRP3A and DRP3B are recruited to the outer mitochondrial membrane and form a contractible ring (Arimura *et al.*, 2008; Fujimoto *et al.*, 2009). DRP3A and DRP3B isoforms co-localise to mitochondrial fission sites and to tips of mitochondria after division. Their GTPase activity is required for the mitochondrial fission to proceed (Arimura *et al.*, 2004b; Arimura, 2018). The crystal structure of the human mitochondrial fission dynamin-related protein DNM1L was resolved and current models show a dimer as the basic unit with higher order assemblies (Fröhlich *et al.*, 2013). A current assembly model predicts 48 tetramers (192 monomers) to be required for the formation of a contractible ring around a membrane tubule with a diameter of 0.11 μm (0.35 μm circumference). Assuming similar protein structures and oligomerisation for Arabidopsis DRP3, for a cylindrical-shaped elongated plant mitochondrion with a diameter of 0.4 μm (i.e. half of the 0.8 μm diameter assumed for a normal, spherical mitochondrion) and a resulting circumference of 1.26 μm, 175 tetramers or 700 DRP3 protein copies would be necessary to assemble into a ring around the constriction site (Dataset S2, worksheet #15). As we estimate 67 copies in total for DRP3A and DRP3B per mitochondrion, this could be interpreted as one out of ten mitochondria is undergoing fission at a given time point, under the assumption that DRP3 also forms tetramers in Arabidopsis (Figure 7). This is in line with high fission rates of Arabidopsis mitochondria (Arimura *et al.*, 2004b), and reflects the observation that not every plant mitochondrion displays a constriction site (Arimura *et al.*, 2004a).

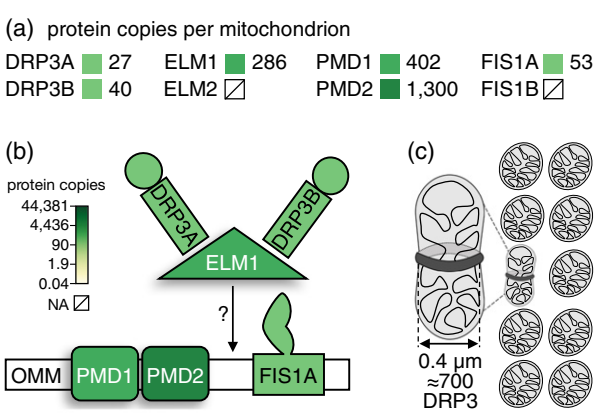

Figure 7. Components of the mitochondrial fission machinery.
(a) Protein copies per mitochondrion of protein species involved in mitochondrial fission. Dynamin-related protein (DRP), elongated mitochondria (ELM), peroxisomal and mitochondrial division factor (PMD), fission (FIS).
(b) Localization and interactions between fission-related proteins. Recruitment of DRP3 isoforms to the outer mitochondrial membrane (OMM) can be ELM1-dependent or -independent (Arimura *et al.*, 2017; Arimura, 2018).
(c) If approximately 700 DRP3 copies are necessary to span a constriction site with a diameter of 0.4 μm, and assuming all DRP3 copies are localized at such a site, the number of DRP3 copies present could support a constriction site at every 10th mitochondrion at a time.

CONCLUSIONS AND OUTLOOK

To gain insights into the makeup and function of individual subcellular compartments, we scaled a quantitative proteomic dataset from isolated Arabidopsis mitochondria to protein copy numbers present in a theoretical single organelle. That enabled us to assess structural and functional features of mitochondria in the context of the geometrical, biochemical and physical constraints of the single organelle. We needed to make several assumptions, and several intrinsic limitations of quantitative proteomics remain. The accuracy of our estimations may be improved in the future through development of the field as well as experimental refinement. Our calculations may then be straightforwardly adjusted and the consequences on the copy numbers and the overall picture revisited. For instance, 5.2% of the protein copies present in the dataset are not functionally annotated (Table S1), which means that the amount of protein copies in the specified functional categories likely represent underestimations. Despite all required caution, the picture that several of our thought experiments deliver is generally consistent with conclusions drawn independently from

previous experimental analyses. This provides confidence that our assumptions are reasonable, and that the approach is valid and informative overall.

We provide an innovative and coherent perspective of how a plant mitochondrion works and are able to deduce unanticipated details of mitochondrial biology. By combining quantitative proteomics with cell biology, we exemplify insights into the local environment that a mitochondrial protein might encounter and provide quantitative estimates to further define the roles that individual protein species, families or complexes play as part of the individual mitochondrion. Although we cover diverse examples of mitochondrial function and organisation, we regard the dataset as a resource to be exploited by the community and encourage our colleagues to make use of it for specific questions and thought experiments.

A single mitochondrion only contains an estimated amount of about 80 fg of protein (Dataset S1, worksheet #2). Hence, assessing the proteome of a single mitochondrion directly is currently technically not feasible. Our approach provides an indirect alternative, but does not allow any insight into the potential heterogeneity between mitochondria with respect to their size, metabolic state or biochemical makeup. Overcoming technical sensitivity limitations would allow an assessment of the differences between individual single mitochondrial proteomes. Heterogeneity in mitochondrial populations likely carries biological significance, especially for those proteins present at very low or even substoichiometric copy numbers. Micromanipulation- or MALDI imaging-based approaches to resolve individual mitochondria may provide an avenue for proteins with larger copy numbers and favourable properties for mass spectrometry analysis (Yajima *et al.*, 2018; Zhang *et al.*, 2018). Innovative single cell proteomic approaches and single molecule approaches, such as nanopore sequencing of proteins (Budnik *et al.*, 2018; Restrepo-Pérez *et al.*, 2018) may open the door to the first single organelle proteomes with quantitative protein coverage.

EXPERIMENTAL PROCEDURES

Cultivation of a heterotrophic Arabidopsis cell suspension culture and isolation of mitochondria

A heterotrophic Arabidopsis cell suspension culture was established as described previously (Sunderhaus *et al.*, 2006; Schikowsky *et al.*, 2017). Cells were sub-cultured on a weekly basis after which their mass increased by a factor of three. Mitochondria isolations were performed after 7 days of culture and used a combination of differential centrifugation and isopycnic Percoll (GE Healthcare, Solingen, Germany; https://www.gelifesciences.com/en/de/shop/cell-therapy/media/percoll-density-gradient-media-p-05823) gradient centrifugation as described by Werhahn *et al.* (2001). Isolated mitochondria were washed, pelleted and re-suspended to yield a concentration of 100 mg mitochondria per mL and stored at −80°C. Four independent mitochondria isolations were performed.

Mass spectrometry

For each mitochondria isolation, a volume corresponding to 50 μg of protein (according to Bradford) was mixed with the same volume of 2x Laemmli buffer (125 mM Tris HCl [pH 6.8], 4% [w/v] SDS, 10% [v/v] β-mercaptoethanol, 0.1% [w/v] bromophenol blue). Solubilized proteins were purified, concentrated, and digested in a glycine-SDS gel. The resulting peptides were subsequently extracted as previously described (Thal *et al.*, 2018) and resuspended in 20 μl of 5% [v/v] ACN, 0.1% [v/v] TFA. LC-MS/MS was primarily performed as described in (Thal *et al.*, 2018) with minor differences. Peptide solution (1 μl) was loaded on a 2-cm C18 reversed phase trap column (Acclaim PepMap100, diameter: 100 μm, granulometry: 5 μm, pore size: 100 Å; Thermo Fisher Scientific, Waltham, MA, USA; https://www.thermofisher.com/order/catalog/product/164567#/164567) and further separated on a 50-cm C18 reversed phase analytical column (Acclaim PepMap100, diameter: 75 μm, granulometry: 3 μm, pore size: 100 Å; Thermo Fisher Scientific). Peptides were eluted by a non-linear 5–36% [v/v] acetonitrile gradient in 0.1% [v/v] formic acid over a period of 240 min at 33°C.

Processing of MS data

Acquired LC-MS/MS spectra were queried against an in-house modified TAIR10 database comprising protein models of the mitochondrial and plastid genomes after RNA editing using MaxQuant 1.6.0.1 (Cox and Mann, 2008). Editing site information was based on the PREPACT database (Lenz *et al.*, 2018) and a published RNA-seq analysis (Bentolila *et al.*, 2013). Sites that are edited at more than 50% efficiency were considered. The search parameters were set to: carbamidomethylation (C) as fixed modification, oxidation (M) and acetylation (protein N-term) as variable modifications. The specific digestion mode was set to trypsin (P) and a maximum of two missed cleavage sites was allowed. FDR at the protein and PSM level was set to 1%. For maximum proteome coverage, the minimum number of unique peptides per protein group was 1. Unique and razor peptides were used for protein quantification. The iBAQ function of MaxQuant was enabled, "log fit" disabled.

To increase the number of quantifiable proteins between the four replicates, we used retention time alignment and peptide identification transfer via the "match between runs" feature of MaxQuant with a match time windows of 0.7 min and an alignment time window of 20 min (Cox *et al.*, 2014).

Estimating the average single mitochondrion protein inventory

The considerations are provided in the Results section and the calculations are detailed in Dataset S1 (worksheet #2). In brief, the volume and mass of a mitochondrion of 0.8 μm in diameter was calculated assuming a spherical shape and a mitochondrial density of 1.2 g ml^{-1} (Glas and Bahr, 1966). Of the mitochondrial mass 25% were considered protein. Total protein mass was divided by the mass of the abundance-adjusted average mitochondrial protein to calculate the total protein copies per mitochondrion. The copy number of each individual protein species was estimated by multiplying the normalized median iBAQ score with the total protein copies.

DATA STATEMENT

The mass spectrometry proteomics data are openly accessible. They have been deposited to the ProteomeXchange Consortium via the PRIDE partner repository (Vizcaino *et al.*, 2013) with the dataset identifier PXD014292.

ACKNOWLEDGEMENTS

We thank Michael Senkler (Hannover) for excellent bioinformatics support. We further thank Ian Max Møller (Aarhus) and José Gualberto (Strasbourg), as well as both anonymous reviewers for critical reading and very helpful comments that have strengthened this manuscript. This work was enabled through the collaborative DFG research grant PAK918 (EU54/4-1, IF1655/3-1, MA2379/14-1, MU4137/1-1, SCHA1953/3-1, SCHW1719/5-1) as part of the 'Plant Mitochondria in New Light' initiative.

CONFLICT OF INTEREST

The authors declare no conflict of interest.

AUTHOR CONTRIBUTIONS

H-PB, PF and MS conceived the project in active discussion with all co-authors. HE and NR performed the itochondrial isolations, the proteomic experiments, and nalyzed the proteomic data. IF advised on MaxQuant ata search and iBAQ evaluation. PF performed the scaling to protein copy numbers with input from MS, H-PB, HE, SJMS and EHM. All co-authors contributed to the writing of the individual sections including individual data analyses. The first draft of the manuscript was assembled by PF, EHM, SJMS and MS. All co-authors contributed to finalizing the manuscript.

SUPPORTING INFORMATION

Additional Supporting Information may be found in the online version of this article.

Figure S1. Characteristics of the proteomic dataset.

Figure S2. Copy numbers of proteins involved in plant mitochondrial protein import and sorting.

Table S1. Functional sub-categories for 917 proteins with mitochondrial localisation as identified based on SUBAcon.

Dataset S1. Proteomic dataset and calculation of protein copy numbers.

Dataset S2. Calculations for specific examples discussed.

Dataset S3. Subsets of proteins discussed in the individual sections.

REFERENCES

Altmann, R. (1890) *Die Elementarorganismen und ihre Beziehungen zu den Zellen*. 1st ed. Leipzig: Veit. Available at: http://www.deutschestextarchiv.de/book/show/altmann_elementarorganismen_1890.

Andrés-Colás, N., Zhu, Q., Takenaka, M., De Rybel, B., Weijers, D. and Van Der Straeten, D. (2017) Multiple PPR protein interactions are involved in the RNA editing system in *Arabidopsis* mitochondria and plastids. *Proc. Natl Acad. Sci. USA*, **114**, 8883–8888.

Arike, L., Valgepea, K., Peil, L., Nahku, R., Adamberg, K. and Vilu, R. (2012) Comparison and applications of label-free absolute proteome quantification methods on *Escherichia coli*. *J. Proteomics*, **75**, 5437–5448.

Arimura, S. (2018) Fission and fusion of plant mitochondria, and genome maintenance. *Plant Physiol.* **176**, 152–161.

Arimura, S., Aida, G.P., Fujimoto, M., Nakazono, M. and Tsutsumi, N. (2004a) *Arabidopsis* dynamin-like protein 2a (ADL2a), like ADL2b, is involved in plant mitochondrial division. *Plant Cell Physiol.* **45**, 236–242.

Arimura, S., Yamamoto, J., Aida, G.P., Nakazono, M. and Tsutsumi, N. (2004b) Frequent fusion and fission of plant mitochondria with unequal nucleoid distribution. *Proc. Natl Acad. Sci. USA*, **101**, 7805–7808.

Arimura, S., Fujimoto, M., Doniwa, Y., Kadoya, N., Nakazono, M., Sakamoto, W. and Tsutsumi, N. (2008) Arabidopsis ELONGATED MITOCHONDRIA1 is required for localization of DYNAMIN-RELATED PROTEIN3A to mitochondrial fission sites. *Plant Cell*, **20**, 1555–1566.

Arimura, S.-I., Kurisu, R., Sugaya, H., Kadoya, N. and Tsutsumi, N. (2017) Cold treatment induces transient mitochondrial fragmentation in *Arabidopsis thaliana* in a way that requires DRP3A but not ELM1 or an ELM1-like homologue, ELM2. *Int. J. Mol. Sci.* **18**, 2161.

Backert, S., Lurz, R., Oyarzabal, O.A. and Börner, T. (1997) High content, size and distribution of single-stranded DNA in the mitochondria of *Chenopodium album* (L.). *Plant Mol. Biol.* **33**, 1037–1050.

Barkan, A. and Small, I. (2014) Pentatricopeptide repeat proteins in plants. *Annu. Rev. Plant Biol.* **65**, 415–442.

Bauer, M.F., Sirrenberg, C., Neupert, W. and Brunner, M. (1996) Role of Tim23 as voltage sensor and presequence receptor in protein import into mitochondria. *Cell*, **87**, 33–41.

Bauwe, H. and Kolukisaoglu, Ü. (2003) Genetic manipulation of glycine decarboxylation. *J. Exp. Bot.* **54**, 1523–1535.

Bauwe, H., Hagemann, M. and Fernie, A.R. (2010) Photorespiration: players, partners and origin. *Trends Plant Sci.* **15**, 330–336.

Bayrhuber, M., Meins, T., Habeck, M. *et al.* (2008) Structure of the human voltage-dependent anion channel. *Proc. Natl Acad. Sci. USA*, **105**, 15370–15375.

Bentolila, S., Oh, J., Hanson, M.R. and Bukowski, R. (2013) Comprehensive high-resolution analysis of the role of an *Arabidopsis* gene family in RNA editing. *PLoS Genet.* **9**, e1003584.

Berthet, J. and Baudhuin, P. (1967) A remark about the determination of the water content of mitochondria. *J. Cell Biol.* **34**, 701–702.

Blum, T.B., Hahn, A., Meier, T., Davies, K.M. and Kühlbrandt, W. (2019) Dimers of mitochondrial ATP synthase induce membrane curvature and self-assemble into rows. *Proc. Natl Acad. Sci. USA*, **116**, 4250–4255.

Bourguignon, J., Macherel, D., Neuburger, M. and Douce, R. (1992) Isolation, characterization, and sequence analysis of a cDNA clone encoding L-protein, the dihydrolipoamide dehydrogenase component of the glycine cleavage system from pea-leaf mitochondria. *Eur. J. Biochem.* **204**, 865–873.

Bourguignon, J., Vauclare, P., Merand, V., Forest, E., Neuburger, M. and Douce, R. (1993) Glycine decarboxylase complex from higher plants. Molecular cloning, tissue distribution and mass spectrometry analyses of the T protein. *Eur. J. Biochem.* **217**, 377–386.

Bourguignon, J., Merand, V., Rawsthorne, S., Forest, E. and Douce, R. (1996) Glycine decarboxylase and pyruvate dehydrogenase complexes share the same dihydrolipoamide dehydrogenase in pea leaf mitochondria: evidence from mass spectrometry and primary-structure analysis. *Biochem. J.* **313**, 229–234.

Bowker-Kinley, M. and Popov, K.M. (1999) Evidence that pyruvate dehydrogenase kinase belongs to the ATPase/kinase superfamily. *Biochem. J.* **344**, 47–53.

Brown, G.G., Colas des Francs-Small, C. and Ostersetzer-Biran, O. (2014) Group II intron splicing factors in plant mitochondria. *Front. Plant Sci.* **5**, 35.

Bubulya, P.A. and Spector, D.L. (2004) On the movements of nuclear components in living cells. *Exp. Cell Res.* **296**, 4–11.

Budnik, B., Levy, E., Harmange, G. and Slavov, N. (2018) SCoPE-MS: mass spectrometry of single mammalian cells quantifies proteome heterogeneity during cell differentiation. *Genome Biol.* **19**, 161.

Cappadocia, L., Parent, J.-S., Zampini, É., Lepage, É., Sygusch, J. and Brisson, N. (2012) A conserved lysine residue of plant Whirly proteins is necessary for higher order protein assembly and protection against DNA damage. *Nucleic Acids Res.* **40**, 258–269.

Chen, Q., Jin, C., Shao, X. *et al.* (2018) Super-resolution tracking of mitochondrial dynamics with an Iridium(III) luminophore. *Small*, **14**, e1802166.

Cheng, S., Gutmann, B., Zhong, X. *et al.* (2016) Redefining the structural motifs that determine RNA binding and RNA editing by pentatricopeptide repeat proteins in land plants. *Plant J.* **85**, 532–547.

Chew, O., Whelan, J. and Millar, A.H. (2003) Molecular definition of the ascorbate-glutathione cycle in *Arabidopsis* mitochondria reveals dual targeting of antioxidant defenses in plants. *J. Biol. Chem.* **278**, 46869–46877.

Chow, K.-S., Singh, D.P., Roper, J.M. and Smith, A.G. (1997) A single precursor protein for ferrochelatase-I from *Arabidopsis* is imported *in vitro* into both chloroplasts and mitochondria. *J. Biol. Chem.* **272**, 27565–27571.

Chow, K.S., Singh, D.P., Walker, A.R. and Smith, A.G. (1998) Two different genes encode ferrochelatase in *Arabidopsis*: mapping, expression and subcellular targeting of the precursor proteins. *Plant J.* **15**, 531–541.

Colombini, M. (2004) VDAC: the channel at the interface between mitochondria and the cytosol. *Mol. Cell. Biochem.* **256–257**, 107–115.

Cowdry, E.V. (1924) Mitochondria, Golgi apparatus and chromidial substance. In *General Cytology* (Cowdry, E.V., ed). Chicago, IL: The University of Chicago Press, pp. 311–382.

Cox, M.M. (2007) Motoring along with the bacterial RecA protein. *Nat. Rev. Mol. Cell Biol.* **8**, 127–138.

Cox, J. and Mann, M. (2008) MaxQuant enables high peptide identification rates, individualized p.p.b.-range mass accuracies and proteome-wide protein quantification. *Nat. Biotechnol.* **26**, 1367–1372.

Cox, J., Hein, M.Y., Luber, C.A., Paron, I., Nagaraj, N. and Mann, M. (2014) Accurate proteome-wide label-free quantification by delayed normalization and maximal peptide ratio extraction, termed MaxLFQ. *Mol. Cell Proteomics*, **13**, 2513–2526.

Davies, K.M., Anselmi, C., Wittig, I., Faraldo-Gomez, J.D. and Kühlbrandt, W. (2012) Structure of the yeast F1Fo-ATP synthase dimer and its role in shaping the mitochondrial cristae. *Proc. Natl Acad. Sci. USA*, **109**, 13602–13607.

Dudkina, N.V., Heinemeyer, J., Keegstra, W., Boekema, E.J. and Braun, H.-P. (2005) Structure of dimeric ATP synthase from mitochondria: an angular association of monomers induces the strong curvature of the inner membrane. *FEBS Lett.* **579**, 5769–5772.

Dudkina, N.V., Kudryashev, M., Stahlberg, H. and Boekema, E.J. (2011) Interaction of complexes I, III, and IV within the bovine respirasome by single particle cryoelectron tomography. *Proc. Natl Acad. Sci. USA*, **108**, 15196–15200.

El Zawily, A.M., Schwarzländer, M., Finkemeier, I. *et al.* (2014) FRIENDLY regulates mitochondrial distribution, fusion, and quality control in *Arabidopsis*. *Plant Physiol.* **166**, 808–828.

Engel, N., van den Daele, K., Kolukisaoglu, U., Morgenthal, K., Weckwerth, W., Parnik, T., Keerberg, O. and Bauwe, H. (2007) Deletion of glycine decarboxylase in *Arabidopsis* is lethal under nonphotorespiratory conditions. *Plant Physiol.* **144**, 1328–1335.

Engel, N., Ewald, R., Gupta, K.J., Zrenner, R., Hagemann, M. and Bauwe, H. (2011) The presequence of *Arabidopsis* serine hydroxymethyltransferase SHM2 selectively prevents import into mesophyll mitochondria. *Plant Physiol.* **157**, 1711–1720.

Eubel, H., Heinemeyer, J. and Braun, H.P. (2004) Identification and characterization of respirasomes in potato mitochondria. *Plant Physiol.* **134**, 1450–1459.

Eubel, H., Lee, C.P., Kuo, J., Meyer, E.H., Taylor, N.L. and Millar, A.H. (2007) Free-flow electrophoresis for purification of plant mitochondria by surface charge: isolation of plant mitochondria by FFE. *Plant J.* **52**, 583–594.

Fabre, B., Lambour, T., Bouyssié, D., Menneteau, T., Monsarrat, B., Burlet-Schiltz, O. and Bousquet-Dubouch, M.-P. (2014) Comparison of label-free quantification methods for the determination of protein complexes subunits stoichiometry. *EuPA Open Proteomics*, **4**, 82–86.

Fessl, T., Watkins, D., Oatley, P. *et al.* (2018) Dynamic action of the Sec machinery during initiation, protein translocation and termination. *eLife*, **7**, e35112.

Finkemeier, I. and Schwarzländer, M. (2018) Mitochondrial regulation and signalling in the photosynthetic cell: principles and concepts. In *Annual Plant Reviews online*. (Roberts, J.A., ed). Chichester, UK: John Wiley & Sons Ltd, pp. 185–226.

Finkemeier, I., Goodman, M., Lamkemeyer, P., Kandlbinder, A., Sweetlove, L.J. and Dietz, K.-J. (2005) The mitochondrial type II peroxiredoxin F is essential for redox homeostasis and root growth of *Arabidopsis thaliana* under stress. *J. Biol. Chem.* **280**, 12168–12180.

Fröhlich, C., Grabiger, S., Schwefel, D., Faelber, K., Rosenbaum, E., Mears, J., Rocks, O. and Daumke, O. (2013) Structural insights into oligomerization and mitochondrial remodelling of dynamin 1-like protein. *EMBO J.* **32**, 1280–1292.

Fromm, S., Braun, H.-P. and Peterhänsel, C. (2016a) Mitochondrial gamma carbonic anhydrases are required for complex I assembly and plant reproductive development. *New Phytol.* **211**, 194–207.

Fromm, S., Senkler, J., Zabaleta, E., Peterhänsel, C. and Braun, H.-P. (2016b) The carbonic anhydrase domain of plant mitochondrial complex I. *Physiol. Plantarum*, **157**, 289–296.

Fujimoto, M., Arimura, S., Mano, S. *et al.* (2009) *Arabidopsis* dynamin-related proteins DRP3A and DRP3B are functionally redundant in mitochondrial fission, but have distinct roles in peroxisomal fission. *Plant J.* **58**, 388–400.

Ghifari, A.S., Huang, S. and Murcha, M.W. (2019) The peptidases involved in plant mitochondrial protein import. *J. Exp. Bot.* https://doi.org/10.1093/jxb/erz365

Glas, U. and Bahr, G.F. (1966) Quantitative study of mitochondria in rat liver: dry mass, wet mass, volume, and concentration of solids. *J. Cell Biol.* **29**, 507–523.

Gold, V.A.M., Ieva, R., Walter, A., Pfanner, N., van der Laan, M. and Kühlbrandt, W. (2014) Visualizing active membrane protein complexes by electron cryotomography. *Nat. Commun.* **5**, 4129.

Gualberto, J.M. and Kühn, K. (2014) DNA-binding proteins in plant mitochondria: implications for transcription. *Mitochondrion*, **19**, 323–328.

Gualberto, J.M. and Newton, K.J. (2017) Plant mitochondrial genomes: dynamics and mechanisms of mutation. *Annu. Rev. Plant Biol.* **68**, 225–252.

Guillaumot, D., Lopez-Obando, M., Baudry, K. *et al.* (2017) Two interacting PPR proteins are major *Arabidopsis* editing factors in plastid and mitochondria. *Proc. Natl Acad. Sci. USA*, **114**, 8877–8882.

Gupte, S., Wu, E.S., Hoechli, L., Hoechli, M., Jacobson, K., Sowers, A.E. and Hackenbrock, C.R. (1984) Relationship between lateral diffusion, collision frequency, and electron transfer of mitochondrial inner membrane oxidation-reduction components. *Proc. Natl Acad. Sci. USA*, **81**, 2606–2610.

Hagedorn, P.H., Flyvbjerg, H. and Møller, I.M. (2004) Modelling NADH turnover in plant mitochondria. *Physiol. Plant.* **120**, 370–385.

Hahn, A., Parey, K., Bublitz, M., Mills, D.J., Zickermann, V., Vonck, J., Kühlbrandt, W. and Meier, T. (2016) Structure of a complete ATP synthase dimer reveals the molecular basis of inner mitochondrial membrane morphology. *Mol. Cell*, **63**, 445–456.

Halliwell, B. and Gutteridge, J.M.C. (2015) *Free Radicals in Biology and Medicine*. New York, NY: Oxford University Press.

Hartl, M. and Finkemeier, I. (2012) Plant mitochondrial retrograde signaling: post-translational modifications enter the stage. *Front. Plant Sci.* **3**, 253.

Hasse, D., Mikkat, S., Thrun, H.-A., Hagemann, M. and Bauwe, H. (2007) Properties of recombinant glycine decarboxylase P- and H-protein subunits from the cyanobacterium *Synechocystis* sp. strain PCC 6803. *FEBS Lett.* **581**, 1297–1301.

Hatzfeld, Y., Maruyama, A., Schmidt, A., Noji, M., Ishizawa, K. and Saito, K. (2000) β-Cyanoalanine synthase is a mitochondrial cysteine synthase-like protein in spinach and *Arabidopsis*. *Plant Physiol.* **123**, 1163–1172.

Heazlewood, J.L., Tonti-Filippini, J.S., Gout, A.M., Day, D.A., Whelan, J. and Millar, A.H. (2004) Experimental analysis of the *Arabidopsis* mitochondrial proteome highlights signaling and regulatory components, provides assessment of targeting prediction programs, and indicates plant-specific mitochondrial proteins. *Plant Cell*, **16**, 241–256.

Hey, D., Ortega-Rodes, P., Fan, T., Schnurrer, F., Brings, L., Hedtke, B. and Grimm, B. (2016) Transgenic tobacco lines expressing sense or antisense FERROCHELATASE 1 RNA show modified ferrochelatase activity in roots and provide experimental evidence for dual localization of ferrochelatase 1. *Plant Cell Physiol.* **57**, 2576–2585.

Hildebrandt, T.M., Nunes Nesi, A., Araújo, W.L. and Braun, H.-P. (2015) Amino acid catabolism in plants. *Mol. Plant*, **8**, 1563–1579.

Hodge, T. and Colombini, M. (1997) Regulation of metabolite flux through voltage-gating of VDAC channels. *J. Membr. Biol.* **157**, 271–279.

Hoitzing, H., Johnston, I.G. and Jones, N.S. (2015) What is the function of mitochondrial networks? A theoretical assessment of hypotheses and proposal for future research. *Bioessays*, **37**, 687–700.

Hooper, C.M., Tanz, S.K., Castleden, I.R., Vacher, M.A., Small, I.D. and Millar, A.H. (2014) SUBAcon: a consensus algorithm for unifying the subcellular localization data of the *Arabidopsis* proteome. *Bioinformatics*, **30**, 3356–3364.

Hosp, F., Lassowskat, I., Santoro, V. *et al.* (2017) Lysine acetylation in mitochondria: from inventory to function. *Mitochondrion*, **33**, 58–71.

Hsu, J.L., Hsieh, Y., Tu, C., O'Connor, D., Nick, H.S. and Silverman, D.N. (1996) Catalytic properties of human manganese superoxide dismutase. *J. Biol. Chem.* **271**, 17687–17691.

Huang, S., Van Aken, O., Schwarzländer, M., Belt, K. and Millar, A.H. (2016) The roles of mitochondrial reactive oxygen species in cellular signaling and stress response in plants. *Plant Physiol.* **171**, 1551–1559.

Hüdig, M., Maier, A., Scherrers, I., Seidel, L., Jansen, E.E.W., Mettler-Altmann, T., Engqvist, M.K.M. and Maurino, V.G. (2015) Plants possess a cyclic mitochondrial metabolic pathway similar to the mammalian metabolic repair mechanism involving malate dehydrogenase and L-2-hydroxyglutarate dehydrogenase. *Plant Cell Physiol.* **56**, 1820–1830.

Ito, J., Taylor, N.L., Castleden, I., Weckwerth, W., Millar, A.H. and Heazlewood, J.L. (2009) A survey of the *Arabidopsis thaliana* mitochondrial phosphoproteome. *Proteomics*, **9**, 4229–4240.

Jakobs, S. and Wurm, C.A. (2014) Super-resolution microscopy of mitochondria. *Curr. Opin. Chem. Biol.* **20**, 9–15.

Kingsbury, B.F. (1912) Cytoplasmic fixation. *Anat. Rec.* **6**, 39–52.

Kitajima, S., Kurioka, M., Yoshimoto, T., Shindo, M., Kanaori, K., Tajima, K. and Oda, K. (2008) A cysteine residue near the propionate side chain of heme is the radical site in ascorbate peroxidase. *FEBS J.* **275**, 470–480.

Kliebenstein, D.J., Monde, R.A. and Last, R.L. (1998) Superoxide dismutase in *Arabidopsis*: an eclectic enzyme family with disparate regulation and protein localization. *Plant Physiol.* **118**, 637–650.

Klodmann, J., Sunderhaus, S., Nimtz, M., Jansch, L. and Braun, H.P. (2010) Internal architecture of mitochondrial complex I from *Arabidopsis thaliana*. *Plant Cell*, **22**, 797–810.

Kmiec, B., Teixeira, P.F. and Glaser, E. (2014) Shredding the signal: targeting peptide degradation in mitochondria and chloroplasts. *Trends Plant Sci.* **19**, 771–778.

Köhler, D., Schmidt-Gattung, S. and Binder, S. (2010) The DEAD-box protein PMH2 is required for efficient group II intron splicing in mitochondria of *Arabidopsis thaliana*. *Plant Mol. Biol.* **72**, 459–467.

König, A.-C., Hartl, M., Boersema, P.J., Mann, M. and Finkemeier, I. (2014a) The mitochondrial lysine acetylome of *Arabidopsis*. *Mitochondrion*, **19**, 252–260.

König, A.-C., Hartl, M., Pham, P.A. *et al.* (2014b) The *Arabidopsis* class II sirtuin is a lysine deacetylase and interacts with mitochondrial energy metabolism. *Plant Physiol.* **164**, 1401–1414.

Krauss, S. (2001) Mitochondria: structure and role in respiration. *Encyclopedia Life Sci.* 1–6.

Krey, J.F., Wilmarth, P.A., Shin, J.-B., Klimek, J., Sherman, N.E., Jeffery, E.D., Choi, D., David, L.L. and Barr-Gillespie, P.G. (2014) Accurate label-free protein quantitation with high- and low-resolution mass spectrometers. *J. Proteome Res.* **13**, 1034–1044.

Kruft, V., Eubel, H., Jänsch, L., Werhahn, W. and Braun, H.P. (2001) Proteomic approach to identify novel mitochondrial proteins in *Arabidopsis*. *Plant Physiol.* **127**, 1694–1710.

Kühn, K., Richter, U., Meyer, E.H. *et al.* (2009) Phage-type RNA polymerase RPOTmp performs gene-specific transcription in mitochondria of *Arabidopsis thaliana*. *Plant Cell*, **21**, 2762–2779.

Kukat, C., Wurm, C.A., Spahr, H., Falkenberg, M., Larsson, N.-G. and Jakobs, S. (2011) Super-resolution microscopy reveals that mammalian mitochondrial nucleoids have a uniform size and frequently contain a single copy of mtDNA. *Proc. Natl Acad. Sci. USA*, **108**, 13534–13539.

Lenz, H., Hein, A. and Knoop, V. (2018) Plant organelle RNA editing and its specificity factors: enhancements of analyses and new database features in PREPACT 3.0. *BMC Bioinformatics*, **19**, 255.

Lister, R., Chew, O., Rudhe, C., Lee, M.N. and Whelan, J. (2001) *Arabidopsis thaliana* ferrochelatase-I and -II are not imported into *Arabidopsis* mitochondria. *FEBS Lett.* **506**, 291–295.

Liu, M.Y. and Colombini, M. (1992) A soluble mitochondrial protein increases the voltage dependence of the mitochondrial channel, VDAC. *J. Bioenerg. Biomembr.* **24**, 41–46.

Logan, D.C. (2006) Plant mitochondrial dynamics. *Biochim. Biophys. Acta Mol. Cell Res.* **1763**, 430–441.

Logan, D.C. and Leaver, C.J. (2000) Mitochondria-targeted GFP highlights the heterogeneity of mitochondrial shape, size and movement within living plant cells. *J. Exp. Bot.* **51**, 865–871.

Logan, D.C. and Paszkiewicz, G. (2017) The dynamic chondriome: control of number, shape, size and motility of mitochondria. In *Annual Plant Reviews, Volume 50* (Logan, D.C., ed). Chichester, UK: John Wiley & Sons Ltd, pp. 67–109.

Lutziger, I. and Oliver, D.J. (2001) Characterization of two cDNAs encoding mitochondrial lipoamide dehydrogenase from Arabidopsis. *Plant Physiol.* **127**, 615–623.

Mannella, C. (1982) Structure of the outer mitochondrial membrane: ordered arrays of porelike subunits in outer-membrane fractions from *Neurospora crassa* mitochondria. *J. Cell Biol.* **94**, 680–687.

Mannella, C.A. and Bonner, W.D. (1975) X-ray diffraction from oriented outer mitochondrial membranes. Detection of in-plane subunit structure. *Biochim. Biophys. Acta*, **413**, 226–233.

Masuda, T., Suzuki, T., Shimada, H., Ohta, H. and Takamiya, K. (2003) Subcellular localization of two types of ferrochelatase in cucumber. *Planta*, **217**, 602–609.

Maurino, V.G. and Engqvist, M.K.M. (2015) 2-Hydroxy acids in plant metabolism. *Arabidopsis Book*, **13**, e0182.

Maurino, V.G. and Peterhänsel, C. (2010) Photorespiration: current status and approaches for metabolic engineering. *Curr. Opin. Plant Biol.* **13**, 248–255.

McClung, C.R., Hsu, M., Painter, J.E., Gagne, J.M., Karlsberg, S.D. and Salomé, P.A. (2000) Integrated temporal regulation of the photorespiratory pathway. Circadian regulation of two *Arabidopsis* genes encoding serine hydroxymethyltransferase. *Plant Physiol.* **123**, 381–392.

Meyer, E.H., Heazlewood, J.L. and Millar, A.H. (2007) Mitochondrial acyl carrier proteins in *Arabidopsis thaliana* are predominantly soluble matrix proteins and none can be confirmed as subunits of respiratory complex I. *Plant Mol. Biol.* **64**, 319–327.

Meyer, E.H., Welchen, E. and Carrie, C. (2019) Assembly of the complexes of the oxidative phosphorylation system in land plant mitochondria. *Annu. Rev. Plant Biol.* **70**, 23–50.

Millar, A.H., Sweetlove, L.J., Giegé, P. and Leaver, C.J. (2001) Analysis of the *Arabidopsis* mitochondrial proteome. *Plant Physiol.* **127**, 1711–1727.

Mlayeh, L., Chatkaew, S., Léonetti, M. and Homblé, F. (2010) Modulation of plant mitochondrial VDAC by phytosterols. *Biophys. J.* **99**, 2097–2106.

Model, K., Meisinger, C. and Kühlbrandt, W. (2008) Cryo-electron microscopy structure of a yeast mitochondrial preprotein translocase. *J. Mol. Biol.* **383**, 1049–1057.

Møller, I.M. (2001) PLANT MITOCHONDRIA AND OXIDATIVE STRESS: electron transport, NADPH turnover, and metabolism of reactive oxygen species. *Annu. Rev. Plant Physiol. Plant Mol. Biol.* **52**, 561–591.

Møller, I.M. (2016) What is hot in plant mitochondria? *Physiol. Plant.* **157**, 256–263.

Mooney, B.P., David, N.R., Thelen, J.J., Miernyk, J.A. and Randall, D.D. (2000) Histidine modifying agents abolish pyruvate dehydrogenase kinase activity. *Biochem. Biophys. Res. Commun.* **267**, 500–503.

Morgenstern, M., Stiller, S.B., Lübbert, P. *et al.* (2017) Definition of a high-confidence mitochondrial proteome at quantitative scale. *Cell Rep.* **19**, 2836–2852.

Mouillon, J.-M., Aubert, S., Bourguignon, J., Gout, E., Douce, R. and Rébeillé, F. (1999) Glycine and serine catabolism in non-photosynthetic higher plant cells: their role in C1 metabolism: role of glycine and serine in C1 metabolism. *Plant J.* **20**, 197–205.

Mueller, S.J., Lang, D., Hoernstein, S.N.W. *et al.* (2014) Quantitative analysis of the mitochondrial and plastid proteomes of the moss *Physcomitrella patens* reveals protein macrocompartmentation and microcompartmentation. *Plant Physiol.* **164**, 2081–2095.

Murchie, E.H. and Lawson, T. (2013) Chlorophyll fluorescence analysis: a guide to good practice and understanding some new applications. *J. Exp. Bot.* **64**, 3983–3998.

Murphy, M.P. (2009) How mitochondria produce reactive oxygen species. *Biochem. J.* **417**, 1–13.

Nelson, C.J., Li, L., Jacoby, R.P. and Millar, A.H. (2013) Degradation rate of mitochondrial proteins in *Arabidopsis thaliana* cells. *J. Proteome Res.* **12**, 3449–3459.

Ohnishi, T. and Hagihara, B. (1964) Preparation of yeast mitochondria. *J. Biochem.* **55**, 584–585.

Oldenkott, B., Yang, Y., Lesch, E., Knoop, V. and Schallenberg-Rüdinger, M. (2019) Plant-type pentatricopeptide repeat proteins with a DYW domain drive C-to-U RNA editing in *Escherichia coli*. *Commun. Biol.* **2**, 85.

Oliver, D.J., Neuburger, M., Bourguignon, J. and Douce, R. (1990) Interaction between the component enzymes of the glycine decarboxylase multienzyme complex. *Plant Physiol.* **94**, 833–839.

Parsons, J.A. (1965) Mitochondrial incorporation of tritiated thymidine in *Tetrahymena pyriformis*. *J. Cell Biol.* **25**, 641–645.

Pebay-Peyroula, E., Dahout-Gonzalez, C., Kahn, R., Trézéguet, V., Lauquin, G.J.-M. and Brandolin, G. (2003) Structure of mitochondrial ADP/ATP carrier in complex with carboxyatractyloside. *Nature*, **426**, 39–44.

Pérez-Ortín, J.E., Alepuz, P.M. and Moreno, J. (2007) Genomics and gene transcription kinetics in yeast. *Trends Genet.* **23**, 250–257.

Pérez-Ruiz, J.M., Naranjo, B., Ojeda, V., Guinea, M. and Cejudo, F.J. (2017) NTRC-dependent redox balance of 2-Cys peroxiredoxins is needed for optimal function of the photosynthetic apparatus. *Proc. Natl Acad. Sci. USA*, **114**, 12069–12074.

Peterhänsel, C., Horst, I., Niessen, M., Blume, C., Kebeish, R., Kürkcüoglu, S. and Kreuzaler, F. (2010) Photorespiration. *Arabidopsis Book*, **8**, e0130.

Preuten, T., Cincu, E., Fuchs, J., Zoschke, R., Liere, K. and Börner, T. (2010) Fewer genes than organelles: extremely low and variable gene copy numbers in mitochondria of somatic plant cells: gene copy numbers in mitochondria. *Plant J.* **64**, 948–959.

Puntarulo, S., Sánchez, R.A. and Boveris, A. (1988) Hydrogen peroxide metabolism in soybean embryonic axes at the onset of germination. *Plant Physiol.* **86**, 626–630.

Qian, Y. and Johnson, K.A. (2017) The human mitochondrial single-stranded DNA-binding protein displays distinct kinetics and thermodynamics of DNA binding and exchange. *J. Biol. Chem.* **292**, 13068–13084.

Rafelski, S.M. (2013) Mitochondrial network morphology: building an integrative, geometrical view. *BMC Biol.* **11**, 71.

Ramírez-Aguilar, S.J., Keuthe, M., Rocha, M., Fedyaev, V.V., Kramp, K., Gupta, K.J., Rasmusson, A.G., Schulze, W.X. and van Dongen, J.T. (2011) The composition of plant mitochondrial supercomplexes changes with oxygen availability. *J. Biol. Chem.* **286**, 43045–43053.

Reichheld, J.P., Khafif, M., Riondet, C., Droux, M., Bonnard, G. and Meyer, Y. (2007) Inactivation of thioredoxin reductases reveals a complex interplay between thioredoxin and glutathione pathways in *Arabidopsis* development. *Plant Cell*, **19**, 1851–1865.

Restrepo-Pérez, L., Joo, C. and Dekker, C. (2018) Paving the way to single-molecule protein sequencing. *Nat. Nanotechnol.* **13**, 786–796.

Rugen, N., Straube, H., Franken, L.E., Braun, H.-P. and Eubel, H. (2019a) Complexome profiling reveals association of PPR proteins with ribosomes in the mitochondria of plants. *Mol. Cell. Proteomics.* **18**, 1345–1362.

Rugen, N., Straube, H., Franken, L.E., Braun, H.-P. and Eubel, H. (2019b) Correction: complexome profiling reveals association of PPR proteins with ribosomes in the mitochondria of plants. *Mol. Cell. Proteomics.* **18**, 1704.

Salvato, F., Havelund, J.F., Chen, M., Rao, R.S.P., Rogowska-Wrzesinska, A., Jensen, O.N., Gang, D.R., Thelen, J.J. and Møller, I.M. (2014) The potato tuber mitochondrial proteome. *Plant Physiol.* **164**, 637–653.

Schikowsky, C., Senkler, J. and Braun, H.-P. (2017) SDH6 and SDH7 contribute to anchoring succinate dehydrogenase to the inner mitochondrial membrane in *Arabidopsis thaliana*. *Plant Physiol.* **173**, 1094–1108.

Schwanhäusser, B., Busse, D., Li, N., Dittmar, G., Schuchhardt, J., Wolf, J., Chen, W. and Selbach, M. (2011) Global quantification of mammalian gene expression control. *Nature*, **473**, 337–342.

Schwarzländer, M., Logan, D.C., Johnston, I.G., Jones, N.S., Meyer, A.J., Fricker, M.D. and Sweetlove, L.J. (2012) Pulsing of membrane potential in individual mitochondria: a stress-induced mechanism to regulate respiratory bioenergetics in *Arabidopsis*. *Plant Cell*, **24**, 1188–1201.

Schwerzmann, K., Cruz-Orive, L.M., Eggman, R., Sänger, A. and Weibel, E.R. (1986) Molecular architecture of the inner membrane of mitochondria from rat liver: a combined biochemical and stereological study. *J. Cell Biol.* **102**, 97–103.

Scott, I. and Logan, D.C. (2011) Mitochondrial dynamics. In *Plant Mitochondria* (Kempken, F., ed.). New York, NY: Springer New York, pp. 31–63.

Senkler, J., Senkler, M., Eubel, H. *et al.* (2017) The mitochondrial complexome of *Arabidopsis thaliana*. *Plant J.* **89**, 1079–1092.

Sheahan, M.B., Rose, R.J. and McCurdy, D.W. (2004) Organelle inheritance in plant cell division: the actin cytoskeleton is required for unbiased inheritance of chloroplasts, mitochondria and endoplasmic reticulum in dividing protoplasts. *Plant J.* **37**, 379–390.

Sheahan, M.B., McCurdy, D.W. and Rose, R.J. (2005) Mitochondria as a connected population: ensuring continuity of the mitochondrial genome during plant cell dedifferentiation through massive mitochondrial fusion. *Plant J.* **44**, 744–755.

Shedge, V., Arrieta-Montiel, M., Christensen, A.C. and Mackenzie, S.A. (2007) Plant mitochondrial recombination surveillance requires unusual RecA and MutS homologs. *Plant Cell*, **19**, 1251–1264.

Sirrenberg, C., Endres, M., Becker, K., Bauer, M.F., Walther, E., Neupert, W. and Brunner, M. (1997) Functional cooperation and stoichiometry of protein translocases of the outer and inner membranes of mitochondria. *J. Biol. Chem.* **272**, 29963–29966.

Sjostrand, F.S. (1953) Electron microscopy of mitochondria and cytoplasmic double membranes. *Nature*, **171**, 30–32.

Somerville, C.R. and Ogren, W.L. (1981) Photorespiration-deficient mutants of *Arabidopsis thaliana* lacking mitochondrial serine transhydroxymethylase activity. *Plant Physiol.* **67**, 666–671.

de Souza, W., Attias, M. and Rodrigues, J.C.F. (2009) Particularities of mitochondrial structure in parasitic protists (Apicomplexa and Kinetoplastida). *Int. J. Biochem. Cell Biol.* **41**, 2069–2080.

Sun, F., Huo, X., Zhai, Y., Wang, A., Xu, J., Su, D., Bartlam, M. and Rao, Z. (2005) Crystal structure of mitochondrial respiratory membrane protein complex II. *Cell*, **121**, 1043–1057.

Sun, T., Bentolila, S. and Hanson, M.R. (2016) The unexpected diversity of plant organelle RNA editosomes. *Trends Plant Sci.* **21**, 962–973.

Sun, Y., Wollman, A., Huang, F., Leake, M. and Liu, L. (2019) Single-organelle quantification reveals the stoichiometric and structural variability of carboxysomes dependent on the environment. *Plant Cell*, **31**, 1648–1664.

Sunderhaus, S., Dudkina, N.V., Jänsch, L., Klodmann, J., Heinemeyer, J., Perales, M., Zabaleta, E., Boekema, E.J. and Braun, H.-P. (2006) Carbonic anhydrase subunits form a matrix-exposed domain attached to the membrane arm of mitochondrial complex I in plants. *J. Biol. Chem.* **281**, 6482–6488.

Sweetlove, L.J., Heazlewood, J.L., Herald, V., Holtzapffel, R., Day, D.A., Leaver, C.J. and Millar, A.H. (2002) The impact of oxidative stress on *Arabidopsis* mitochondria. *Plant J.* **32**, 891–904.

Sweetlove, L.J., Beard, K.F.M., Nunes-Nesi, A., Fernie, A.R. and Ratcliffe, R.G. (2010) Not just a circle: flux modes in the plant TCA cycle. *Trends Plant Sci.* **15**, 462–470.

Takenaka, M., Zehrmann, A., Verbitskiy, D., Kugelmann, M., Härtel, B. and Brennicke, A. (2012) Multiple organellar RNA editing factor (MORF) family proteins are required for RNA editing in mitochondria and plastids of plants. *Proc. Natl Acad. Sci. USA*, **109**, 5104–5109.

Tanaka, R. and Tanaka, A. (2007) Tetrapyrrole biosynthesis in higher plants. *Annu. Rev. Plant Biol.* **58**, 321–346.

Taylor, N.L., Heazlewood, J.L. and Millar, A.H. (2011) The Arabidopsis thaliana 2-D gel mitochondrial proteome: refining the value of reference maps for assessing protein abundance, contaminants and post-translational modifications. *Proteomics*, **11**, 1720–1733.

Thal, B., Braun, H.-P. and Eubel, H. (2018) Proteomic analysis dissects the impact of nodulation and biological nitrogen fixation on *Vicia faba* root nodule physiology. *Plant Mol. Biol.* **97**, 233–251.

Tronconi, M.A., Fahnenstich, H., Gerrard Weehler, M.C., Andreo, C.S., Flügge, U.-I., Drincovich, M.F. and Maurino, V.G. (2008) *Arabidopsis* NAD-malic enzyme functions as a homodimer and heterodimer and has a major impact on nocturnal metabolism. *Plant Physiol.* **146**, 1540–1552.

Tronconi, M.A., Maurino, V.G., Andreo, C.S. and Drincovich, M.F. (2010) Three different and tissue-specific NAD-malic enzymes generated by alternative subunit association in *Arabidopsis thaliana*. *J. Biol. Chem.* **285**, 11870–11879.

Uhrig, R.G., Labandera, A.-M., Tang, L.-Y., Sieben, N.A., Goudreault, M., Yeung, E., Gingras, A.-C., Samuel, M.A. and Moorhead, G.B.G. (2017) Activation of mitochondrial protein phosphatase SLP2 by MIA40 regulates seed germination. *Plant Physiol.* **173**, 956–969.

Utter, M.F., Keech, D.B. and Nossal, P.M. (1958) Oxidative phosphorylation by subcellular particles from yeast. *Biochem. J.* **68**, 431–440.

Vaseghi, M.-J., Chibani, K., Telman, W., Liebthal, M.F., Gerken, M., Schnitzer, H., Mueller, S.M. and Dietz, K.-J. (2018) The chloroplast 2-cysteine peroxiredoxin functions as thioredoxin oxidase in redox regulation of chloroplast metabolism. *eLife*, **7**, e38194.

Vincent, A.E., White, K., Davey, T. *et al.* (2019) Quantitative 3D mapping of the human skeletal muscle mitochondrial network. *Cell Rep.* **27**, 321.

de Virville, J.D., Alin, M.-F., Aaron, Y., Rémy, R., Guillot-Salomon, T. and Cantrel, C. (1998) Changes in functional properties of mitochondria during growth cycle of *Arabidopsis thaliana* cell suspension cultures. *Plant Physiol. Biochem.* **36**, 347–356.

Vizcaino, J.A., Cote, R.G., Csordas, A. *et al.* (2013) The Proteomics Identifications (PRIDE) database and associated tools: status in 2013. *Nucleic Acids Res.* **41**, D1063–D1069.

Vogel, U. and Jensen, K.F. (1994) The RNA chain elongation rate in *Escherichia coli* depends on the growth rate. *J. Bacteriol.* **176**, 2807–2813.

Wagner, S., Behera, S., De Bortoli, S. *et al.* (2015) The EF-hand Ca^{2+} binding protein MICU choreographs mitochondrial Ca^{2+} dynamics in *Arabidopsis*. *Plant Cell*, **27**, 3190–3212.

Waltz, F., Nguyen, T.-T., Arrivé, M. *et al.* (2019) Small is big in *Arabidopsis* mitochondrial ribosome. *Nat. Plants*, **5**, 106–117.

Wang, Q., Fristedt, R., Yu, X., Chen, Z., Liu, H., Lee, Y., Guo, H., Merchant, S.S. and Lin, C. (2012) The gamma-carbonic anhydrase subcomplex of mitochondrial complex I is essential for development and important for photomorphogenesis of *Arabidopsis*. *Plant Physiol.* **160**, 1373–1383.

Weiss, H., von Jagow, G., Klingenberg, M. and Bücher, T. (1970) Characterization of *Neurospora crassa* mitochondria prepared with a grind-mill. *Eur. J. Biochem.* **14**, 75–82.

Werhahn, W., Niemeyer, A., Jänsch, L., Kruft, V., Schmitz, U.K. and Braun, H. (2001) Purification and characterization of the preprotein translocase of the outer mitochondrial membrane from *Arabidopsis*. Identification of multiple forms of TOM20. *Plant Physiol.* **125**, 943–954.

Werner, S. and Neupert, W. (1972) Functional and biogenetical heterogeneity of the inner membrane of rat-liver mitochondria. *Eur. J. Biochem.* **25**, 379–396.

van Wijk, K.J., Friso, G., Walther, D. and Schulze, W.X. (2014) Meta-analysis of *Arabidopsis thaliana* phospho-proteomics data reveals compartmentalization of phosphorylation motifs. *Plant Cell*, **26**, 2367–2389.

Wirtz, M., Beard, K.F.M., Lee, C.P. *et al.* (2012) Mitochondrial cysteine synthase complex regulates O-acetylserine biosynthesis in plants. *J. Biol. Chem.* **287**, 27941–27947.

Woodson, J.D., Perez-Ruiz, J.M. and Chory, J. (2011) Heme synthesis by plastid ferrochelatase I regulates nuclear gene expression in plants. *Curr. Biol.* **21**, 897–903.

Wurm, C.A., Neumann, D., Lauterbach, M.A., Harke, B., Egner, A., Hell, S.W. and Jakobs, S. (2011) Nanoscale distribution of mitochondrial import receptor Tom20 is adjusted to cellular conditions and exhibits an inner-cellular gradient. *Proc. Natl Acad. Sci. USA*, **108**, 13546–13551.

Yajima, Y., Hiratsuka, T., Kakimoto, Y., Ogawa, S., Shima, K., Yamazaki, Y., Yoshikawa, K., Tamaki, K. and Tsuruyama, T. (2018) Region of interest analysis using mass spectrometry imaging of mitochondrial and sarcomeric proteins in acute cardiac infarction tissue. *Sci. Rep.* **8**, 7493.

Yasuda, R., Noji, H., Yoshida, M., Kinosita, K. and Itoh, H. (2001) Resolution of distinct rotational substeps by submillisecond kinetic analysis of F1-ATPase. *Nature*, **410**, 898–904.

Zaegel, V., Guermann, B., Le Ret, M., Andrés, C., Meyer, D., Erhardt, M., Canaday, J., Gualberto, J.M. and Imbault, P. (2006) The plant-specific ssDNA binding protein OSB1 is involved in the stoichiometric transmission of mitochondrial DNA in *Arabidopsis*. *Plant Cell*, **18**, 3548–3563.

Zamponi, N., Zamponi, E., Cannas, S.A., Billoni, O.V., Helguera, P.R. and Chialvo, D.R. (2018) Mitochondrial network complexity emerges from fission/fusion dynamics. *Sci. Rep.* **8**, 363.

Zhang, Z., Huang, L., Shulmeister, V.M., Chi, Y.I., Kim, K.K., Hung, L.W., Crofts, A.R., Berry, E.A. and Kim, S.H. (1998) Electron transfer by domain movement in cytochrome bc1. *Nature*, **392**, 677–684.

Zhang, Y., Sun, K., Sandoval, F.J., Santiago, K. and Roje, S. (2010) One-carbon metabolism in plants: characterization of a plastid serine hydroxymethyltransferase. *Biochem. J.* **430**, 97–105.

Zhang, Y., Beard, K.F.M., Swart, C. *et al.* (2017) Protein-protein interactions and metabolite channelling in the plant tricarboxylic acid cycle. *Nat. Commun.* **8**, 15212.

Zhang, L., Khattar, N., Kemenes, I., Kemenes, G., Zrinyi, Z., Pirger, Z. and Vertes, A. (2018) Subcellular peptide localization in single identified neurons by capillary microsampling mass spectrometry. *Sci. Rep.* **8**, 12227.

Zhou, Z.H., McCarthy, D.B., O'Connor, C.M., Reed, L.J. and Stoops, J.K. (2001) The remarkable structural and functional organization of the eukaryotic pyruvate dehydrogenase complexes. *Proc. Natl Acad. Sci. USA*, **98**, 14802–14807.

Zickermann, V., Wirth, C., Nasiri, H., Siegmund, K., Schwalbe, H., Hunte, C. and Brandt, U. (2015) Mechanistic insight from the crystal structure of mitochondrial complex I. *Science*, **347**, 44–49.

Zizi, M., Forte, M., Blachly-Dyson, E. and Colombini, M. (1994) NADH regulates the gating of VDAC, the mitochondrial outer membrane channel. *J. Biol. Chem.* **269**, 1614–1616.